study. The stimuli were composed of a 0.1-msec plus segment, a 0.1-msec minus segment, and alternating polarity outputs. Generally, the ABR waveforms were recorded for 12.8 msec at a sampling rate of 40,000 Hz using 50–5,000 Hz band-pass filter settings, and the waveforms from 256 stimuli at a frequency of 9 Hz were averaged. The ABR waveforms were recorded in 5-dB SPL intervals decreasing from the maximum amplitude until the waveform could no longer be visualized.

Dissection and Sample Preparation

Immediately after 3, 6, 12, or 24 hr or 7, 14, or 28 days after noise exposure, the animals were anesthetized with xylazine (10 mg/g) and ketamine (40 mg/g) and decapitated. The temporal bones were carefully removed from the skull base, and the bulla were opened to expose cochleae. The right cochlea was dissected at the hook using scissors and placed in 750 μl of Trizol Reagent (Invitrogen Corp., Carlsbad, CA) for RNA extraction. The left (or both in several animals) temporal bones were sampled and soaked in 4% paraformaldehyde (PFA) for immunohistochemical analysis (from 0–24 hr post-exposure, $n = 6$;, from 7–28 days post-exposure, $n = 4$; non-exposed control cochlea, $n = 6$). Several right cochleae from 3- or 6-hr post-exposed and non-exposed rats were also sampled for Western blot analysis. The cochlea duct was rapidly dissected using microsurgery. The tissues were then homogenized in ice-cold lysate buffer containing a cocktail of protease inhibitors (Complete, EDTA-free; Roche, Mannheim, Germany), 50 mM of sodium fluoride and 1 mM of sodium orthovanadate. After sonication, the samples were centrifuged at 12,000 rpm for 20 min at 4°C and then stored at −20°C until electrophoresis.

RT-PCR Analysis

Reverse transcriptase reaction with random primers (nonamers) was carried out using a SuperScript III RT-PCR Kit (Invitrogen). The first-strand cDNA was synthesized from 0.5 μg of total RNA. For each PCR experiment, a negative RT control (non-RT RNA) and a negative PCR control (no cDNA template) were also conducted. Second-step RT-PCR was carried out using messageScreen Rat Inflammatory Cytokine Set 2 Multiplex PCR Kits (BioSource International Inc., Camarillo, CA) with 39 cycles of polymerase chain reaction. The thermal cycling conditions of the vendor's protocol for Taq polymerase (Takara Biotechnology Co., Ltd., Otsu, Japan) were followed.

Quantitative real-time RT-PCR reactions were carried out for TNF-α, IL-1β, and IL-6 using Mx3000p (Stratagene, La Jolla, CA). As an internal control, 18S rRNA cDNA was amplified. The TaqMan probes for TNF-α, IL-1β, and IL-6 were all combined with FAM, and those for 18S rRNA were combined with VIC (Applied Biosystems, Foster City, CA). Another fluorescent dye, ROX, was used as a calibrator. The relative expression levels of each cytokine were statistically analyzed using a one-way ANOVA.

Western Blot Analysis

Each sample containing 2.5 μg of protein was subjected to 15% polyacrylamide gel electrophoresis and transferred to a polyvinylidene difluoride membrane. The blots were incubated overnight at 4°C with rabbit anti-IL-6 antibody diluted 1:500 (Sigma, St. Louis, MO), or rabbit anti-IL-6 receptors (IL-6R) antibody (diluted 1:200, Santa Cruz Biotechnology, Santa Cruz, CA). After incubation for 1 hr at room temperature with secondary antibody conjugated with biotin, the blots were incubated with ABC Elite complex (Vectastain ABC Elite Kit; Vector Laboratories Co., Burlingame, CA) and visualized using the ECL Blotting Analysis System (Amersham Bioscience Co., Little Chalfont, UK).

Cryosections and Immunostaining for IL-6

After fixation with 4% PFA, the bony labyrinths were further incubated with Decalcifying Solution A (Plank Rychlo method solution: Wako Pure Chemical Industries, Doshomachi, Osaka, Japan) for 24 hr, dehydrated in a stepwise-manner from 10–30% sucrose, and embedded in Tissue-Tek O.C.T. Compound (Sakura Finetechnical Co., Tokyo, Japan). Series of 6 μm-thick cryosections were then collected onto New Silane II slides (MUTO Pure Chemicals Co., Tokyo, Japan). All of the slides were washed with PBS, incubated in 1.5% hydrogen peroxide for 15 min, rinsed three times in PBS, and incubated in 10% normal goat serum for 1 hr at room temperature and in primary antibodies at 4°C overnight. The primary antibody was the antibody used in the present Western blotting analysis, diluted 1:150. The slides were then incubated in a 1:1,000 dilution of biotinylated secondary antibodies at 37°C for 30 min, washed three times in PBS, then incubated in Elite ABC Kit (Vector Laboratories, Burlingame, CA) for 30 min at room temperature. After a gentle washing in PBS three times, the samples were incubated in diaminobenzidine (DAB) solution (Wako Pure Chemical Industries) for visualization. After washing with PBS, the samples were dehydrated and mounted with cover glasses. The primary antibodies used for the immunofluorescent study were mouse anti-NeuN monoclonal antibody (diluted 1:100, CHEMICON, Temecula, CA) and rabbit anti-IL-6 polyclonal antibody (diluted 1:150). The secondary antibodies were Alexa Fluro (A-11029; Molecular Probes, Eugene, OR) or HRP conjugated antibody (both diluted 1:1,000). The slides were visualized using a TSA-rhodamine visualizing kit (Perkin-Elmer, Boston, MA) according to the manufacture's protocol.

RESULTS

Evaluation of Hearing Impairment Induced by the Noise Exposure

With the noise centered at 4 kHz in a one-octave-wide band of which the peak magnitude was 124 dBSPL (spectrum shown in Fig. 1a.), we produced a noise-induced hearing loss (NIHL) model in the present experiment. The time course of the threshold shift in this model, evaluated using a click-evoked auditory brainstem-evoked response (click ABR), is shown in Figure 1b. The stable threshold shift for up to 3 months suggested that the noise was intense enough to produce a permanent threshold shift (PTS). The final threshold shift level was 41.3 ± 4.27 dB (mean ± SEM) .

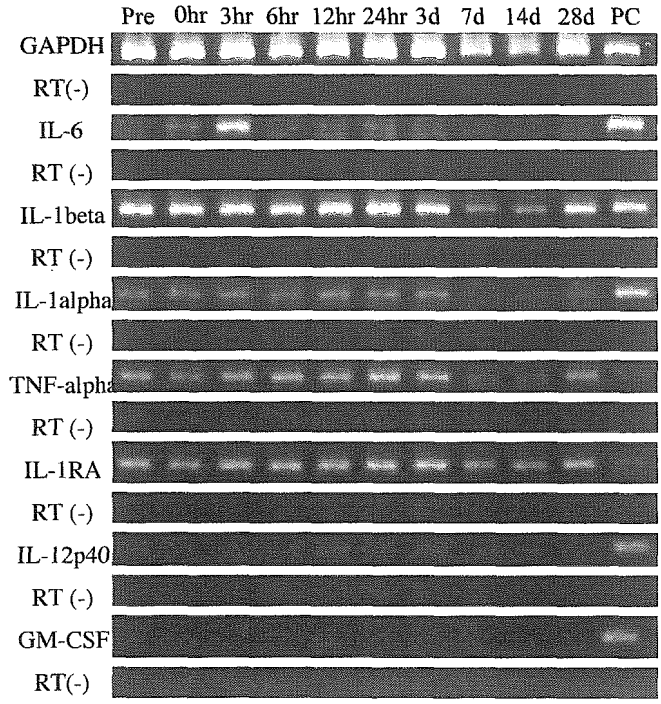

Fig. 2. RT-PCR. Two-step RT-PCR was used to screen for the expression of seven cytokines ($n = 3$). TNF-α, the IL-1 family (IL-1α, β, receptor antagonist), and IL-6, were detected but IL-12 p40 and GM-CSF were not detected. The total RNA quantity in each lane was the same. (PC, positive control; GAPDH, internal control) Note that with unknown reason, the signals at Day 7 and Day 14 of TNF-α, IL-1α, and IL-1β seemed to be low, however, the PCR product of GAPDH at these time-points were also lower than the other time-points.

Transient Upregulation of Proinflammatory Cytokines After Noise Exposure

We carried out a two-step RT-PCR analysis to screen for the expression of cytokines related to inflammation (Fig. 2). Among the seven cytokines that we evaluated, TNF-α, the IL-1 family (IL-1α, β and receptor antagonist). and IL-6 were detected before or after noise exposure. The signals of TNF-α were relatively weak, but detected in a normal state to 28 days after noise exposure. The expressions of IL-1β and IL-1α were detected before and after noise exposure. IL-1RA expression did not change throughout the experiments with or without noise exposure. The expression of IL-6 was detected 0 and 3 hr after noise exposure but then diminished to an undetectable level. IL-12 p40 and GM-CSF expression was not detected.

To assess the precise time-dependent alterations in transcription, we carried out quantitative real-time RT-PCR analyses for TNF-α, IL-1β, and IL-6 using TaqMan probes with 18S rRNA as reference gene. Figure 3 illustrates the expression levels of the RNAs for each cytokine at eight time points after or without noise exposure. Significant IL-1β and IL-6 inductions were detected at 3 hr after exposure ($P < 0.05$, one-way ANOVA). These inductions decreased to the basal level within 24 hr. The same tendency was also observed for TNF-α, whereas no significant differences were detected among the time points.

Western Blot Analysis

We carried out a Western blot analysis to examine IL-6 protein level (Fig. 3d,e). A 27-kDa IL-6 protein was detected as a single band by using an anti-IL-6-specific antibody. Relative upregulation was observed in 3 hr after noise exposure, compared to untreated (i.e., pre-noise) cochleae. After 6 hr, the protein level was significantly upregulated from that for the pre-noise condition. There was no significant difference in the expression of IL-6 receptor (IL-6R) before and after noise exposure (data not shown).

IL-6 Immunostaining After Noise Exposure

To determine which cells produced IL-6, immunohistochemistry for IL-6 was carried out. In pre-noise-exposed cochleae, diffuse weak immunoreactivity was detected in the lateral wall, except for in the stria vascularis. Faintly immunolabeled cells were located in the supra stria region of the lateral wall cells (the area where type V fibrocytes are located) and the spiral prominence (Fig. 4a). At 6 hr after exposure, distinctively immunolabeled cells were observed in the lower part of the cochlea lateral wall cells, including Type III and IV fibrocytes (Fig. 4b). The distribution of IL-6 immunoreactivity was restricted to the cytoplasm of these cells (Fig. 4d,f–h). Among the cochlea turns, a relatively higher immunoreactivity was seen in the apical turn, compared to the basal turn (Fig. 4e). No immunoreactivity was detected without primary antibody incubation (data not shown). Although the IL-6 immunoreactivity was observed in tectorial membrane, we speculate that the staining is background because this region is known to be a high-background area. (Murata et al., 2004; Yamashita et al., 2004).

Figure 5 shows the time-dependent changes in IL-6 immunostaining. Up until 6 hours after noise exposure, the expression pattern became gradually stronger and broader from the lowest part to the higher part of the lateral side of the spiral ligament (Fig. 5a–c). Concomitantly, the IL-6 immunopositive area expanded, from the lateral side toward the medial end of the lateral wall and finally to the damaged stria cells at 12 hr after exposure (Fig. 5b–d).

At 12 and 24 hr after noise exposure, many ganglion cells were immunolabeled for IL-6 in their cytoplasm (Fig. 6d,e), whereas no immunoreactivity was observed within 6 hr (Fig. 6a–c). Diffusely distributed IL-6 immunoreactivity was observed among the ganglion cells (Fig. 6f,g). High-magnification images show the localization of IL-6 and NeuN, a mature neuronal marker. IL-6 immunoreactivity was localized on the surface of some ganglion neurons (Fig. 6h–k,l; arrowheads) and also in the cytoplasm of other neurons (Fig. 6j–l; arrow).

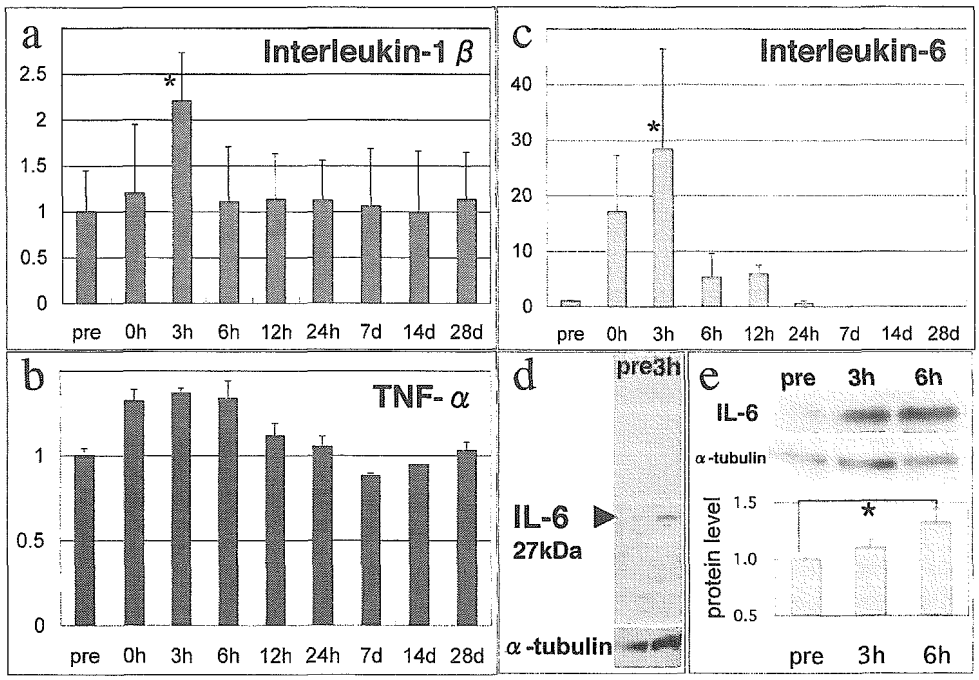

Fig. 3. Quantitative RT-PCR and Western blotting. Quantitative RT-PCR analyses of TNF-α, IL-1β, and IL-6 were carried out using TaqMan probes and 18S rRNA as a reference gene (**a–c**). The amplitude of interleukin-6 RNA expression was the largest of all three cytokines (c). The vertical bar represents the relative ratio of (target gene)/(reference gene). Note that the scales of the vertical bars differ for each target gene. From pre-noise to 24 hr, each $n = 6$; from 7 days to 28 days, each $n = 4$. **d,e:** A whole cochlear Western blotting analysis for IL-6. A single band was detected at the appropriate protein size, demonstrating the high specificity of the IL-6 antibody (d). e: The results of Western blotting for IL-6 at three different time points. A significant difference in IL-6 expression was observed at 6 hr after noise exposure. The vertical bar represents the relative ratio of IL-6 versus α-tubulin (internal control).

DISCUSSION

Proinflammatory cytokines are produced in various organs after tissue damage not only in experimental immune-response models, but also in various types of insults including infection, ischemia, trauma, cryo-ablation, and burns (Berti et al., 2002; Pier et al., 2004), by various types of cells, including residential immune-related cells (such as leukocytes, macrophages, microglia, dendritic cells), neurons and glia in the central nervous system (CNS). We demonstrated that these inflammation-related cytokines were upregulated in noise-induced damaged cochlea and that the time courses of their expressions were very similar to those seen in other traumatized organs. Our data was compatible with the results of several histopathological studies that have pointed out the possibility of inflammatory changes in noise overstimulated cochleae (Hirose et al., 2003, 2005).

In the present study, we demonstrated the induction of IL-6 in lateral wall cells in the early phase of noise-induced cochlear trauma. IL-6 RNA and protein inductions were detected at 3 and 6 hr after noise exposure, respectively. Furthermore, the cytoplasmic expression of IL-6 protein in lateral wall cells appeared in the lower and lateral areas of the spiral ligaments, suggesting that IL-6 protein was newly produced by translation between 3 and 6 hr after noise exposure. Fibrocytes in cochlear lateral wall were anatomically and histologically classified into four (or five; depending on the researchers) subtypes, each of which has particular function (Spicer and Schulte, 1991, 1996). The IL-6 immunoreactive cells in the lower part of lateral wall are interpreted as Type IV and III fibrocytes. Interestingly, we also observed the expression and relative induction of IL-1β and TNF-α before IL-6 RNA expression after noise exposure. Previous reports showed that cochlea lateral wall fibrocytes produce IL-6 when stimulated by IL-1β and TNF-α in vitro (Ichimiya et al., 2003). Based on the findings of this and former reports, we speculate that IL-6 may be produced in vivo in cochleae, initially by Type IV and III fibrocytes via the synergetic stimulation of IL-1β and TNF-α. Activated microglia and monocytes have been known to produce cytokines in other damaged organs, including brain injuries (Allan and Rothwell, 2001; Lo et al., 2003). Our data clearly demonstrated that the IL-6-expressing cells were not colocalized with Iba-1-positive cells in this area (Iba-1 is a specific marker for activated macrophages or monocytes). Therefore, we concluded that the IL-6 expression observed in this study was not by activated immune-related cells, like homing macrophages or microglia.

In addition, a double-labeling study showed the presence of IL-6 expression in NeuN-positive neurons of the spiral ganglion at 12–24 hr after noise exposure, although not all of the NeuN-positive neurons expressed IL-6. IL-6 induction in the spiral ganglion neurons might

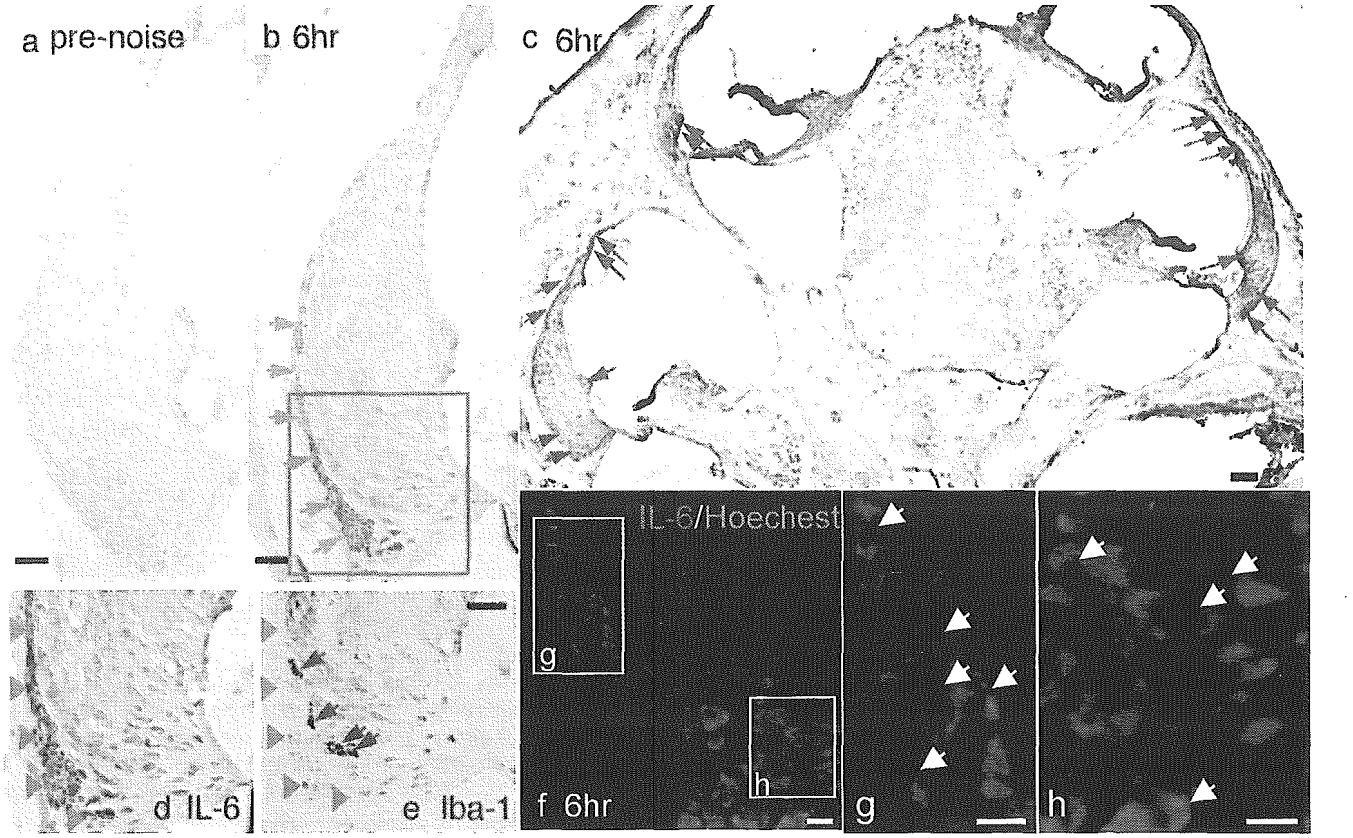

Fig. 4. Immunostaining of IL-6. Immunohistochemistry of interleukin-6 in the noise-exposed cochleae. At 6 hr after exposure, prominent IL-6 immunoreactivity was found in the lateral side of the spiral ligament (orange arrows in **b**, blue arrows in **c**, orange arrowheads in **d**). IL-6 immunoreactivity was distributed in the cytoplasm of the lateral wall cells. Morphologically, these cells include Type III and IV fibrocytes (arrows in b–d,**g**,**h**). d,**e**: Serial sections. IL-6 expression (orange arrows in d) was not colocalized with Iba-1 (red arrows in e), an activated macrophage or microglia marker. Note that IL-6 was not expressed in the stria vascularis at this time point. **a**: Control cochlea b–h: 6 hr after noise exposure. a–d: IL-6, e: Iba-1, **f**–h: red, IL-6; blue, Hoechst 33432. Scale bars = a–e, 50 μm; f–I, 20 μm.

reflect the second peak of IL-6 RNA production observed 12 and 24 hr after noise exposure. In the CNS, mature neurons produce IL-6 in response to various cellular stresses, including ischemia and excitotoxic stress (Suzuki et al., 1999; Acarin et al., 2000; Block et al., 2000). Our data suggest IL-6 production in the spiral ganglion neurons may also due to cellular stresses, including noise overstimulation, because overstimulation of hair cells induces a secondary degeneration in spiral ganglion (Lim, 1976; Webster and Webster, 1981).

IL-6 is an intercellular signaling molecule via paracrine or autocrine manners. One of the roles of IL-6 is its anti-oxidative stress effect by upregulating several anti-apoptotic genes, including bcl-family, or cell survival signals (Lin et al., 2001). Another role is regulating inflammation including immune responses. Knock-out mice study has shown that, in cryo-ablated brain, the loss of IL-6 production suppresses macrophage recruitment and decreases local inflammation, but increases apoptosis in injured cells (Morganti-Kossmann et al., 2002).

The localization of diffuse IL-6 immunoreactivity in damaged cochleae should be crucial. In the lateral wall, IL-6 immunoreactivity was observed initially in and around Type IV fibrocytes; then expanded diffusely and broadly toward the stria cells. In the spiral ganglion, IL-6 immunoreactivity was seen not only in the cytoplasm, but also on the cell surface of neurons. Lateral wall fibrocytes and stria cells are crucially important for generating endocochlear potential (EP) and ion transportation, both of which are indispensable for auditory hair cells to generate action potential in response to sound stimuli (Spicer and Schulte, 1996; Crouch et al., 1997; Flagella et al., 1999; Kikuchi et al., 2000). These cells are susceptible to noise-induced overstimulation, and among them, Type IV fibrocytes are the most susceptible cells, which undergo apoptotic degeneration and never repopulate (Hirose and Liberman, 2003). Taking all these data together, our data suggest the possibility that Type IV fibrocytes might be the initiator of the local inflammatory response against the stress in cochlea.

Several published reports suggested that the involvement of IL-1 family and TNF-α in damaged cochleae (Komeda et al., 1999; Satoh et al., 2002; Wang et al., 2003). Although the mechanism and function of these

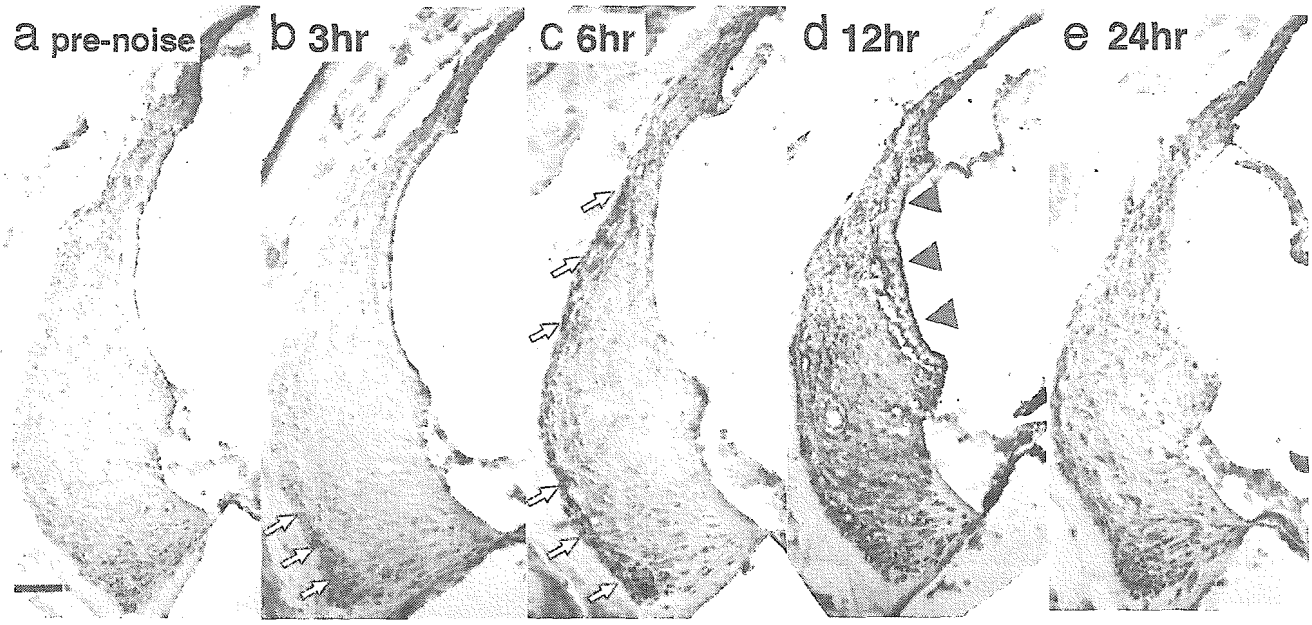

Fig. 5. Time-dependent expression of IL-6 in the lateral wall of the cochlear basal turn. At 3 hr after exposure, moderately immunolabeled cells were found in the lowest region of the lateral wall, where Type IV fibrocytes are located (**b**). At 6 hr after noise exposure, IL-6 immunoreactive cells had increased markedly, expanding from the lowest region to the higher region of the lateral side of the wall (white arrows) (**c**). From 3–12 hr after exposure, IL-6 immunoreactive area broadened from lateral to medial and finally extended to the swollen, vacuolizing stria cells (**d**, arrowheads). The diffuse IL-6-positive area had mostly disappeared at 24 hr after noise exposure (**e**). In the spiral prominence and supra-stria fibrocytes, weak immunoreactivity was detected from pre-noise to 24 hr after noise exposure. **a:** control cochlea; b–e: 3, 6, 12, 24 hr after noise exposure. Scale bar = 50 μm.

cytokines in NIHL are still obscure, suppression of infiltration of inflammatory cells into cochleae by inhibiting TNF-α signal has been demonstrated to reduce hearing loss in experimental inner ear inflammation model (Satoh et al., 2002; Wang et al., 2003). Our present data led us to believe that inhibition of IL-6 signal in the acute phase of NIHL would also be a therapeutic strategy. Therapeutic interventions against acute inflammation by targeting IL-6 have been tried, but two loss-of-function analyses in examining CNS injuries reported opposite results: the blockage of IL-6 signaling in spinal cord injury ameliorated functional recovery (Okada et al., 2004), whereas the same treatment aggravated cerebral damage in an experimental cerebral ischemia model (Yamashita et al., 2005). These results indicate that the expression of IL-6 acts as a double-edged sword in the CNS, and the function of IL-6 is context-dependent, presumably depending largely on the type of cells and the type of stresses. The biological meaning of IL-6 expression in noise-induced hearing loss remains unclear. Although it might be a self-protecting mechanism against exposure to large amounts of sounds, excessive expression would worsen long-term cochlear function. In the latter case, the expression of IL-6 in the early phase could be a therapeutic target of artificial manipulations, similar to the strategies that have been used for spinal cord injuries or rheumatoid arthritis (Ito et al., 2004; Nishimoto et al., 2005; Yokota et al., 2005). Thus, a loss-of-function analysis is critically important and should be attempted in NIHL model in the near future.

This is the first study demonstrating the induction of proinflammatory cytokines in noise-exposed cochleae. Clinically, appropriate doses of steroid-based therapy have been chosen for many years as a favorable option for preventing long-term cochlear function in patients with acoustic trauma. The effects of steroid-based treatments against noise-induced hearing loss might be due to an anti-inflammatory reaction, suppressing excessive inflammation. However, large dose of steroids harmed long-term cochlear function by some experimental studies (Karlidag et al., 2002; Takemura et al., 2004). This variable outcome of steroid treatment might be explained by the actions of multifunctional proinflammatory cytokines, like IL-6 whose expression is actually suppressed by steroid treatment in lateral wall fibrocytes in vitro (Maeda et al., 2005). Recent drug-design technology has enabled us to suppress cytokine-mediated inflammation with fewer side effects using non-steroid anti-inflammatory agents, specific inhibitors of each cytokine. For example, in patients with rheumatoid arthritis (RA) or inflammatory bowel disease, the blockage of IL-6 by specific humanized neutralizing antibodies has been clinically used with promising effects (Nishimoto et al., 2004). Our present study suggests the possibility of therapeutic strategies tar-

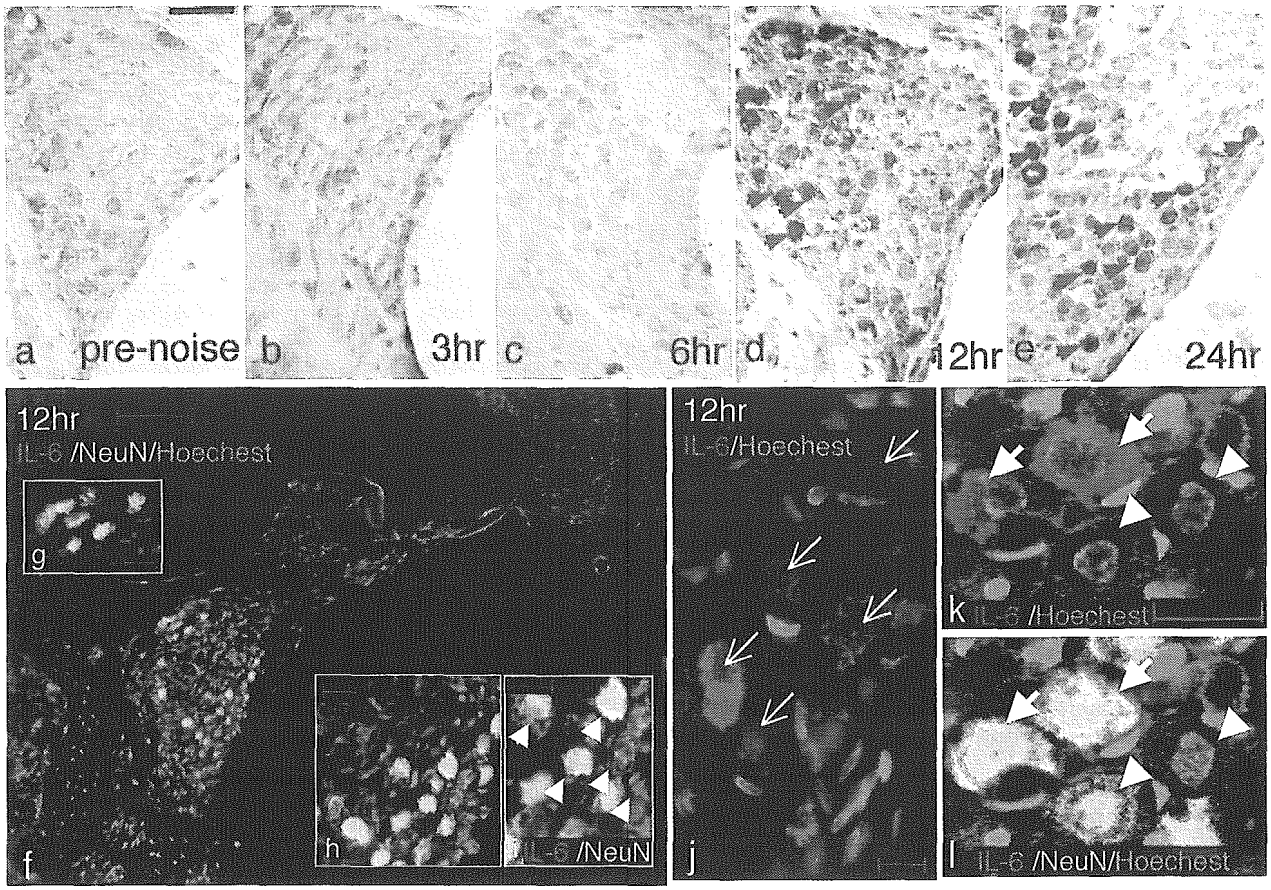

Fig. 6. Time-dependent expression of IL-6 in spiral ganglion after noise overstimulation. In the spiral ganglion, IL-6 immunoreactivity was also observed after noise exposure. The stainings were determined in the spiral ganglion of upper-basal turn of cochleae. The number of IL-6 immunolabeled ganglion cells increased markedly at 12 and 24 hr after noise exposure (**d,e**). **f–i:** Double-immunolabeling for IL-6 (red) and NeuN (green: a mature neuron marker). Higher power photos show IL-6 immunoreactivties on the surface of ganglion cells (h,i,**k,l**; arrowheads) and in the cytoplasm of some ganglion neurons (**j–l**; arrow). **a:** Control cochlea; **b–e:** 3, 6, 12, 24 hr after noise exposure; f–l: 12 hr after noise exposure. Red, IL-6; green, NeuN; blue, Hoechst. k,l: confocal images. Scale bars = a–e, 50 μm; f–l, 20 μm.

geting a specific proinflammatory cytokine, like IL-6, against noise-induced hearing loss.

ACKNOWLEDGMENTS

We are grateful to Dr. K. Dan for detailed instructions and suggestions regarding the RT-PCR and real-time RT-PCR experiments. We are grateful to all of the Okano laboratory's staff, especially to Dr. S. Shibata for critical suggestions regarding immunohistochemistry studies, and to our ENT department colleagues for valuable open discussions. This work was supported by Keio University Grant-in-Aid for Encouragement of Young Medical Scientists, grants from the Japan Science and Technology Agency, Core Research for Evolutional Science and Technology, a Grant-in-Aid for the 21st Century Center of Excellence (COE) program to Keio University from the Japanese Ministry of Education, Culture, Sports, Science and Technology (MEXT), and Grant-in-Aid for Young Scientists (B) to M.F. from the MEXT.

REFERENCES

Acarin L, Gonzalez B, Castellano B. 2000. Neuronal, astroglial and microglial cytokine expression after an excitotoxic lesion in the immature rat brain. Eur J Neurosci 12:3505–3520.

Allan SM, Rothwell NJ. 2001. Cytokines and acute neurodegeneration. Nat Rev Neurosci 2:734–744.

Berti R, Williams AJ, Moffett JR, Hale SL, Velarde LC, Elliott PJ, Yao C, Dave JR, Tortella FC. 2002. Quantitative real-time RT-PCR analysis of inflammatory gene expression associated with ischemia-reperfusion brain injury. J Cereb Blood Flow Metab 22:1068–1079.

Block F, Peters M, Nolden-Koch M. 2000. Expression of IL-6 in the ischemic penumbra. Neuroreport 11:963–967.

Buckley CD, Pilling D, Lord JM, Akbar AN, Scheel-Toellner D, Salmon M. 2001. Fibroblasts regulate the switch from acute resolving to chronic persistent inflammation. Trends Immunol 22:199–204.

Crouch JJ, Sakaguchi N, Lytle C, Schulte BA. 1997. Immunohistochemical localization of the Na-K-Cl co-transporter (NKCC1) in the gerbil inner ear. J Histochem Cytochem 45:773–778.

Flagella M, Clarke LL, Miller ML, Erway LC, Giannella RA, Andringa A, Gawenis LR, Kramer J, Duffy JJ, Doetschman T, Lorenz JN, Yamoah EN, Cardell EL, Shull GE. 1999. Mice lacking the basolateral

Na-K-2Cl cotransporter have impaired epithelial chloride secretion and are profoundly deaf. J Biol Chem 274:26946–26955.

Hashimoto S, Billings P, Harris JP, Firestein GS, Keithley EM. 2005. Innate immunity contributes to cochlear adaptive immune responses. Audiol Neurootol 10:35–43.

Hirose K, Discolo CM, Keasler JR, Ransohoff R. 2005. Mononuclear phagocytes migrate into the murine cochlea after acoustic trauma. J Comp Neurol 489:180–194.

Hirose K, Liberman MC. 2003. Lateral wall histopathology and endocochlear potential in the noise-damaged mouse cochlea. J Assoc Res Otolaryngol 4:339–352.

Hoya N, Okamoto Y, Kamiya K, Fujii M, Matsunaga T. 2004. A novel animal model of acute cochlear mitochondrial dysfunction. Neuroreport 15:1597–1600.

Ichimiya I, Yoshida K, Hirano T, Suzuki M, Mogi G. 2000. Significance of spiral ligament fibrocytes with cochlear inflammation. Int J Pediatr Otorhinolaryngol 56:45–51.

Ichimiya I, Yoshida K, Suzuki M, Mogi G. 2003. Expression of adhesion molecules by cultured spiral ligament fibrocytes stimulated with proinflammatory cytokines. Ann Otol Rhinol Laryngol 112:722–728.

Ito H, Takazoe M, Fukuda Y, Hibi T, Kusugami K, Andoh A, Matsumoto T, Yamamura T, Azuma J, Nishimoto N, Yoshizaki K, Shimoyama T, Kishimoto T. 2004. A pilot randomized trial of a human anti-interleukin-6 receptor monoclonal antibody in active Crohn's disease. Gastroenterology 126:989–996; discussion 947.

Karlidag T, Yalcin S, Ozturk A, Ustundag B, Gok U, Kaygusuz I, Susaman N. 2002. The role of free oxygen radicals in noise induced hearing loss: effects of melatonin and methylprednisolone. Auris Nasus Larynx 29:147–152.

Kikuchi T, Kimura RS, Paul DL, Takasaka T, Adams JC. 2000. Gap junction systems in the mammalian cochlea. Brain Res Brain Res Rev 32:163–166.

Komeda M, Roessler BJ, Raphael Y. 1999. The influence of interleukin-1 receptor antagonist transgene on spiral ganglion neurons. Hear Res 131:1–10.

Lim DJ. 1976. Ultrastructural cochlear changes following acoustic hyperstimulation and ototoxicity. Ann Otol Rhinol Laryngol 85:740–751.

Lin MT, Juan CY, Chang KJ, Chen WJ, Kuo ML. 2001. IL-6 inhibits apoptosis and retains oxidative DNA lesions in human gastric cancer AGS cells through upregulation of anti-apoptotic gene mcl-1. Carcinogenesis 22:1947–1953.

Lo EH, Dalkara T, Moskowitz MA. 2003. Mechanisms, challenges and opportunities in stroke. Nat Rev Neurosci 4:399–415.

Maeda K, Yoshida K, Ichimiya I, Suzuki M. 2005. Dexamethasone inhibits tumor necrosis factor-alpha-induced cytokine secretion from spiral ligament fibrocytes. Hear Res 202:154–160.

Mor A, Abramson SB, Pillinger MH. 2005. The fibroblast-like synovial cell in rheumatoid arthritis: a key player in inflammation and joint destruction. Clin Immunol 115:118–128.

Morganti-Kossmann MC, Rancan M, Stahel PF, Kossmann T. 2002. Inflammatory response in acute traumatic brain injury: a double-edged sword. Curr Opin Crit Care 8:101–105.

Murata J, Murayama A, Horii A, Doi K, Harada T, Okano H, Kubo T. 2004. Expression of Musashi1, a neural RNA-binding protein, in the cochlea of young adult mice. Neurosci Lett 354:201–204.

Nishimoto N, Kanakura Y, Aozasa K, Johkoh T, Nakamura M, Nakano S, Nakano N, Ikeda Y, Sasaki T, Nishioka K, Hara M, Taguchi H, Kimura Y, Kato Y, Asaoku H, Kumagai S, Kodama F, Nakahara H, Hagihara K, Yoshizaki K, Kishimoto T. 2005. Humanized anti-interleukin-6 receptor antibody treatment of multicentric Castleman's disease. Blood 106:2627–2632.

Nishimoto N, Yoshizaki K, Miyasaka N, Yamamoto K, Kawai S, Takeuchi T, Hashimoto J, Azuma J, Kishimoto T. 2004. Treatment of rheumatoid arthritis with humanized anti-interleukin-6 receptor antibody: a multicenter, double-blind, placebo-controlled trial. Arthritis Rheum 50:1761–1769.

Okada S, Nakamura M, Mikami Y, Shimazaki T, Mihara M, Ohsugi Y, Iwamoto Y, Yoshizaki K, Kishimoto T, Toyama Y, Okano H. 2004. Blockade of interleukin-6 receptor suppresses reactive astrogliosis and ameliorates functional recovery in experimental spinal cord injury. J Neurosci Res 76:265–276.

Pier GB, Lyczak JB, Wetzeler LM. 2004. Immunology, infection, and immunity. In: Pier GB, editor. Herndon, VA: American Society for Microbiology.

Satoh H, Firestein GS, Billings PB, Harris JP, Keithley EM. 2002. Tumor necrosis factor-alpha, an initiator, and etanercept, an inhibitor of cochlear inflammation. Laryngoscope 112:1627–1634.

Satoh H, Firestein GS, Billings PB, Harris JP, Keithley EM. 2003. Proinflammatory cytokine expression in the endolymphatic sac during inner ear inflammation. J Assoc Res Otolaryngol 4:139–147.

Shizuki K, Ogawa K, Matsunobu T, Kanzaki J, Ogita K. 2002. Expression of c-Fos after noise-induced temporary threshold shift in the guinea pig cochlea. Neurosci Lett 320:73–76.

Spicer SS, Schulte BA. 1991. Differentiation of inner ear fibrocytes according to their ion transport related activity. Hear Res 56:53–64.

Spicer SS, Schulte BA. 1996. The fine structure of spiral ligament cells relates to ion return to the stria and varies with place-frequency. Hear Res 100:80–100.

Suzuki S, Tanaka K, Nogawa S, Nagata E, Ito D, Dembo T, Fukuuchi Y. 1999. Temporal profile and cellular localization of interleukin-6 protein after focal cerebral ischemia in rats. J Cereb Blood Flow Metab 19:1256–1262.

Takemura K, Komeda M, Yagi M, Himeno C, Izumikawa M, Doi T, Kuriyama H, Miller JM, Yamashita T. 2004. Direct inner ear infusion of dexamethasone attenuates noise-induced trauma in guinea pig. Hear Res 196:58–68.

Wang X, Truong T, Billings PB, Harris JP, Keithley EM. 2003. Blockage of immune-mediated inner ear damage by etanercept. Otol Neurotol 24:52–57.

Webster M, Webster DB. 1981. Spiral ganglion neuron loss following organ of Corti loss: a quantitative study. Brain Res 212:17–30.

Yamashita D, Jiang HY, Schacht J, Miller JM. 2004. Delayed production of free radicals following noise exposure. Brain Res 1019:201–209.

Yamashita T, Sawamoto K, Suzuki S, Suzuki N, Adachi K, Kawase T, Mihara M, Ohsugi Y, Abe K, Okano H. 2005. Blockade of interleukin-6 signaling aggravates ischemic cerebral damage in mice: possible involvement of Stat3 activation in the protection of neurons. J Neurochem 94:459–468.

Yokota S, Miyamae T, Imagawa T, Iwata N, Katakura S, Mori M, Woo P, Nishimoto N, Yoshizaki K, Kishimoto T. 2005. Therapeutic efficacy of humanized recombinant anti-interleukin-6 receptor antibody in children with systemic-onset juvenile idiopathic arthritis. Arthritis Rheum 52:818–825.

Yoshida K, Ichimiya I, Suzuki M, Mogi G. 1999. Effect of proinflammatory cytokines on cultured spiral ligament fibrocytes. Hear Res 137:155–159.

Available online at www.sciencedirect.com
SCIENCE DIRECT
Biochimica et Biophysica Acta 1725 (2005) 57 – 63
BIOCHIMICA ET BIOPHYSICA ACTA
BBA
http://www.elsevier.com/locate/bba

Membranous osteogenesis system modeled with KUSA-A1 mature osteoblasts

Satoshi Matsumoto[a,d], Isao Shibuya[a], Satoshi Kusakari[b], Kaoru Segawa[c], Taro Uyama[a], Akinori Shimada[d], Akihiro Umezawa[a,*]

[a]*Department of Reproductive Biology and Pathology, National Institute for Child Health and Development, 2-10-1 Okura, Setagaya-ku, Tokyo 157-8535, Japan*
[b]*Department of Pathology, Keio University School of Medicine, Tokyo 160-8582, Japan*
[c]*Department of Microbiology and Immunology, Keio University School of Medicine, Tokyo 160-8582, Japan*
[d]*Department of Veterinary Pathology, Tottori University, Tottori 680-8553, Japan*

Received 22 September 2004; received in revised form 16 May 2005; accepted 17 May 2005
Available online 17 June 2005

Abstract

Several stromal cells were established from murine bone marrow cultures. One of the KUSA subclones, KUSA-A1 cells, displays osteogenic characteristics in vitro and in vivo. The calcium deposition, osteocalcin release, and parathyroid hormone (PTH) responsiveness of KUSA-A1 cells indicate that they are mature osteoblasts or osteocytes. Bone had formed in subcutaneous tissue 1 week after subcutaneous injection of cells into immunodeficient mice. The osteogenesis by KUSA-A1 was not mediated by chondrogenesis and thus was considered to be membranous ossification. These unique characteristics of KUSA-A1 cells provide an opportunity to analyze the process of membranous ossification in detail.

Keywords: Membranous osteogenesis; Stromal cell; KUSA; Osteoblast; Gap junction

1. Introduction

The concept of regenerative medicine refers to the cell-mediated restoration of damaged or diseased tissue. Candidate cell sources for tissue regeneration include embryonic stem cells, fetal cells, and adult cells, such as marrow stromal cells [1], each of which has both advantages and drawbacks. Clinical trials with marrow stromal cells have been performed in patients with osteogenesis imperfecta [2] and osteoporosis [3,4], and marrow stromal cells are expected to be a good source of cell therapy [5]. Multipotent mesenchymal stem cells have been isolated from adult marrow and shown to differentiate into multiple cell types, such as osteoblasts, chondrocytes, adipocytes, myoblasts [1,5,6], cardiomyocytes [7,8], endothelial cells, and neuronal cells [9].

In the present study, we characterized a single cloned, immortalized stromal cell line, KUSA-A1, established from murine bone marrow cultures [6]. KUSA-A1 cells are capable of generating mature bone in vivo. They are a unique, mature osteoblast cell line and will serve as a very suitable model for in vivo osteogenesis.

2. Materials and methods

2.1. Cell culture

The stromal cell lines were isolated from long-term bone marrow cultures of C3H/He female mice and cultured as previously described [6,9–11]. Cells were cultured in Iscove's modified Dulbecco's medium (IMDM) supple-

* Corresponding author. Tel.: +81 3 5494 7047; fax: +81 3 5494 7048.
E-mail address: umezawa@1985.jukuin.keio.ac.jp (A. Umezawa).

0304-4165/$ - see front matter © 2005 Elsevier B.V. All rights reserved.
doi:10.1016/j.bbagen.2005.05.027

mented with 20% fetal bovine serum (FBS) and penicillin (100 μg/ml)/streptomycin (250 ng/ml) at 37 °C in humid air with 5% CO_2. Immortalized cells were obtained by frequent subculture for over a year. Cell lines from different dishes were subcloned by limiting dilution. The murine stromal cell lines are summarized in Fig. 1. In vitro calcification assay, osteocalcin production, and evaluation of parathyroid hormone (PTH) response were performed as previously described [10].

2.2. Measurement of alkaline phosphatase (ALP)

KUSA/A1 and MHCTC-E1 cells were analyzed by ALP assay as described [20].

2.3. Communication assay

Intercellular transfer Fluorescent Lucifer Yellow CH (Sigma, St. Louis, Missouri) was measured after the direct microinoculation of the dye into a KUSA-A1 cell as previously described [12,13].

2.4. RNA extraction and Northern blotting

RNA was prepared by homogenizing the specimens in guanidinium isothiocyanate, followed by centrifugation over a cesium chloride cushion as previously described [6,14]. The RNA was then electrophoresed in a 1.0% agarose gel, transferred to a nylon filter, and hybridized with a cDNA insert labeled with ^{32}P-dCTP by the random-primer method at 65 °C for 14–16 h in a buffer containing 5× SSPE (1× SSPE is 0.15 M NaCl, 10 mM NaH_2PO_4/Na_2HPO_4 (pH 7.4), and 1 mM EDTA), 5× Denhardt's solution (1× Denhardt's solution is 0.02% Ficoll polyvinylpyrrolidone and 0.02% BSA), 0.02% poly(A), and 1% SDS. The blots were washed with 2× SSC (1× SSC is 0.15 M NaCl and 0.015 M sodium citrate, pH 7.4) containing 1% SDS at room temperature and 65 °C. Final washing was performed with 0.1× SSC containing 0.1% SDS at 65 °C.

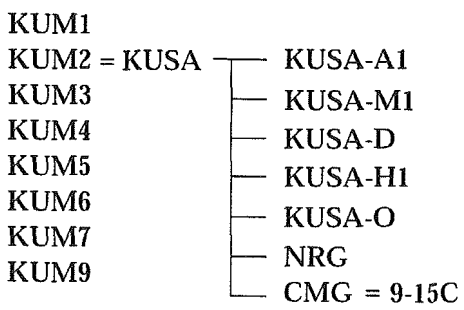

Fig. 1. The murine stromal cell lines. The clonal cells were designated KUM1 [6], KUM2/KUSA [6,9], KUM3-7 [6], and KUM9 [6,9]. The KUSA-A1 [6,11], KUSA-M1 [6], KUSA-D [6], KUSA-H1 [6], KUSA-O [6], and NRG [9] cells were subclones of KUSA cells. The CMG/9-15C cells are a subclone from KUSA cells that had been after exposed to 5-azacytidine [7,11]. The cell names are available at http://1985.jukuin.keio.ac.jp/umezawa/kum/kumh.html.

The blots were exposed to X-ray film at 80 °C with an intensifying screen. RNA blot analysis was carried out as previously described [6,14].

2.5. Transmission electron microscopy (TEM)

KUSA-A1 cells cultured in vitro for 14 days post-confluence were examined by TEM. The samples were fixed in 2.5% glutaraldehyde postfixed in 1% osmium tetroxide. They were rinsed in water, dehydrated, and embedded in epoxy resin. Ultrathin sections (70–90 nm) were cut and stained with 2% uranyl acetate and Reynold's lead citrate before being examined with a JEM-1200 EX microscope (JOEL Co., Japan) at 80 kV.

2.6. Inoculation of cells into mice

To determine the ability of KUSA, KUM3, KUM4, and NIH-3H3 cells to differentiate in vivo, freshly scraped KUSA-MTAg, KUM3-MTAg, KUM4-MTAg, and NIH3T3-MTAg cells (10^7 cells) were subcutaneously inoculated into Balb/c *nu/nu* mice (Sankyo Laboratory, Hamamatsu, Japan) as previously described [6]. Animals were sacrificed by cervical dislocation between 4 and 8 weeks after inoculation.

To determine the potential osteogenic activity of KUSA-A1 cells in vivo, freshly scraped KUSA-A1 cells (10^7 cells) were subcutaneously inoculated into severe combined immunodeficient (SCID) mice (Nippon CLEA, Hamamatsu, Japan). Subcutaneous specimens were resected between 1 and 4 weeks after inoculation and decalcified for a few days in formic acid. The implants were embedded in paraffin. Paraffin sections were deparaffinized, hydrated, and stained with hematoxylin and eosin.

All animals received human care incompliance with the "Principles of Laboratory Animal Care" formulated by the National Society for Medical Research, and the "Guide for the Care and Use of Laboratory Animals" prepared by the Institute of Laboratory Animal Resource and published by the US National Institute of Health (NIH Publication No. 86-23, revised in 1985). The operation protocols were accepted by the Laboratory Animal Care and the Use Committee of the National Research Institute for Child and Health Development, Tokyo, and Keio University School of Medicine.

3. Results

3.1. In vitro characterization of KUSA-A1 cells, single-cell-derived mature osteoblasts

In vitro, calcification by KUSA-A1 cells gradually increased during the culture period (Fig. 2A), and the amount of osteocalcin released into the culture medium also increased (Fig. 2B). The KUSA-A1 cells responded to PTH

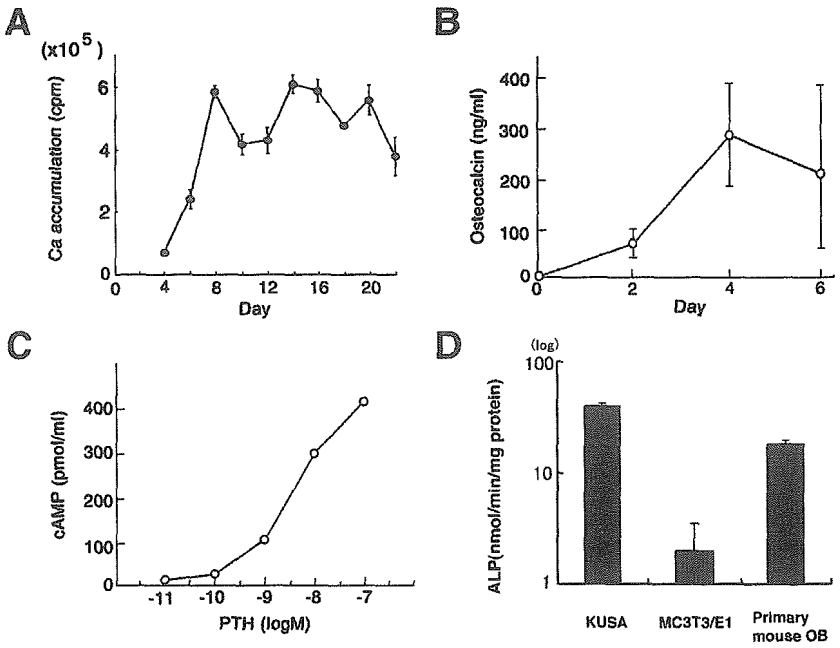

Fig. 2. Characteristics of KUSA-A1 cells as an osteoblast model. (A) Quantitative analysis of calcium deposition by KUSA-A1 cells. (B) Bone Gla protein (Osteocalcin) secretion by KUSA-A1 cells. (C) cAMP production after exposure to PTH. The KUSA-A1 cell response to PTH was assessed by measuring cAMP production. (D) ALP activity in KUSA-A1 cells and MC3T3-E1 cells at 7 days.

in a dose-dependent manner (Fig. 2C). The ALP activity of KUSA-A1 cells was approximately ten-fold higher than in MC3T3-E1 cells at 7 days (Fig. 2D). The calcium deposition and osteocalcin release indicated that KUSA-A1 cells are mature osteoblasts or osteocytes.

3.2. Morphology of KUSA-A1 cells: transmission electron microscopy (TEM) in vitro

Bone nodules [15] that had developed in KUSA-A1 cells cultured in medium supplemented with 10 mM beta-glycerophosphate were fixed and stained in situ by the von Kossa technique (Fig. 3A). The bone nodules consisted of an eosinophilic matrix containing ovoid cells resembling osteocytes, and the KUSA-A1 cells were arranged at the periphery of the nodule in the form of a periosteum-like cell layer. Mineral deposition by the KUSA-A1 cells demonstrated that they have the capacity to differentiate into osteoblasts, to deposit hydroxyapatite in well-developed bone matrix, and to express the differentiated state of osteoblasts.

Ultrastructurally, the matrix was electron-dense and was clearly produced by the cells in the bone nodules (Fig. 3B). The extracellular matrix produced by KUSA-A1 cells was

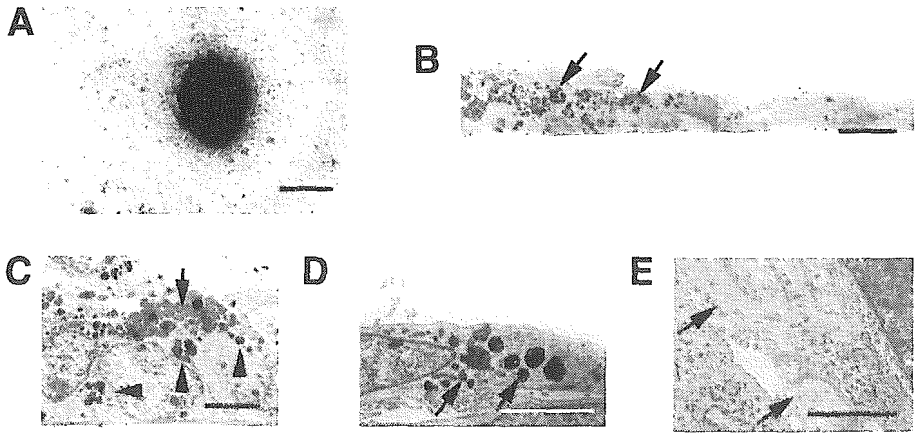

Fig. 3. Ultrastructural analysis of KUSA-A1 cells in culture. (A) KUSA-A1 cells 30 days after confluence. KUSA-A1 cultured in medium supplemented with beta-glycerophosphate was stained in situ by the von Kossa technique. Discrete mineralized nodules are seen. (B) Transmission electron micrograph (TEM) of a nodule present in a KUSA-A1 culture 14 days post-confluence. The extracellular matrix produced by KUSA-A1 cells was observed on the cell surface [arrow]. (C) High-power view of panel B. TEM revealed that the sphere of extracellular matrix produced by KUSA-A1 cells contained a small granular material [arrowhead]. (D) High-power view of a KUSA-A1 cell. Many lysosomal myelin-like figures [arrow] and rough endoplasmic reticulum are seen in its cytoplasm. (E) High-power view of KUSA-A1 cells. Abundant collagen fibrils are visible in the intercellular spaces [arrow], and the cytoplasm contains rough endoplasmic reticulum. Scale bars: 1 mm (A), 20 μm (B), 5 μm (C, D), and 1 μm (E).

observed on the cell surface (Fig. 3C). The cytoplasm of the spindle-shaped cells contained extensive, dilated, and rough endoplasmic reticulum and myelin-like lysosomes (Fig. 3D). Lysosome-rich cells were found in the bone nodules. These cells are probably similar to those observed in vivo [16] and in the primary bone cell cultures [17]. The cells produce abundant, orthogonally oriented collagen fibrils in the intercellular spaces (Fig. 3E), and these fibrils were also found in membrane folds.

3.3. Gap-junctional communication in KUSA-A1 cells

Gap-junctional communication is required for the osteoblast maturation process in culture [18,19], and we used the dye-transfer method to assess the gap-junctional communication between KUSA-A1 cells. When Fluorescent Lucifer Yellow CH was injected into a KUSA-A1 cell, the dye was rapidly transferred to the neighboring cells (Fig. 4A and B), implying that KUSA-A1 cells constitutively communicate with each other via gap junctions.

The expression of gap-junction genes by KUSA cells was investigated by blot hybridization of stromal cell RNA with a connexin 43 cDNA probe. H-1/A of the marrow preadipocyte cell line is a positive control. Distinct 3.0-kb mRNA bands were observed in all of the marrow stromal cell lines when tested with the connexin 43 cDNA probe (Fig. 4C), but no bands were detected in any of the cells when tested with a connexin 32 probe (data not shown).

3.4. Microscopic examination of large subcutaneous masses

NIH3T3, KUM3, KUM4, and KUSA cells transfected with MTAg were designated NIH3T3-MTAg, KUM3-MTAg, KUM4-MTAg, and KUSA-MTAg cells, respectively. Four weeks after subcutaneous inoculation of 10^7 NIH3T3-MTAg, KUM3-MTAg, KUM4-MTAg, KUSA-MTAg, and untransfected KUSA-A1 cells [6] into immunodeficient mice, masses had formed in the subcutaneous tissue. The masses were of three types histologically. Sarcoma-type masses were induced by NIH3T3-MTAg, KUM3-MTAg, and KUM4-MTAg cells and diagnosed as fibrocytic sarcoma; they did not contain bone. The tumors consisted of pleomorphic mesenchymal cells, including multinucleated bizarre giant cells (Fig. 5A and B). The second type of masses was sarcomas with complete bone formation. KUSA-MTAg cells induced sarcomas, most of which contained well-defined complete bone. These sarcomas exhibited an irregular woven pattern of pleomorphic spindle cells that included multinucleated tumor giant cells (Fig. 5C–E). The third type of masses consisted of complete bone and bone cavities with trilineage hematopoiesis. Untransfected KUSA cells formed bone (Fig. 5F–H). Untransfected KUSA-A1 cells, a subclone of the KUSA cells, also formed complete bone 4 weeks after inoculation (Fig. 5I and J). No sarcomatous cell proliferation was observed.

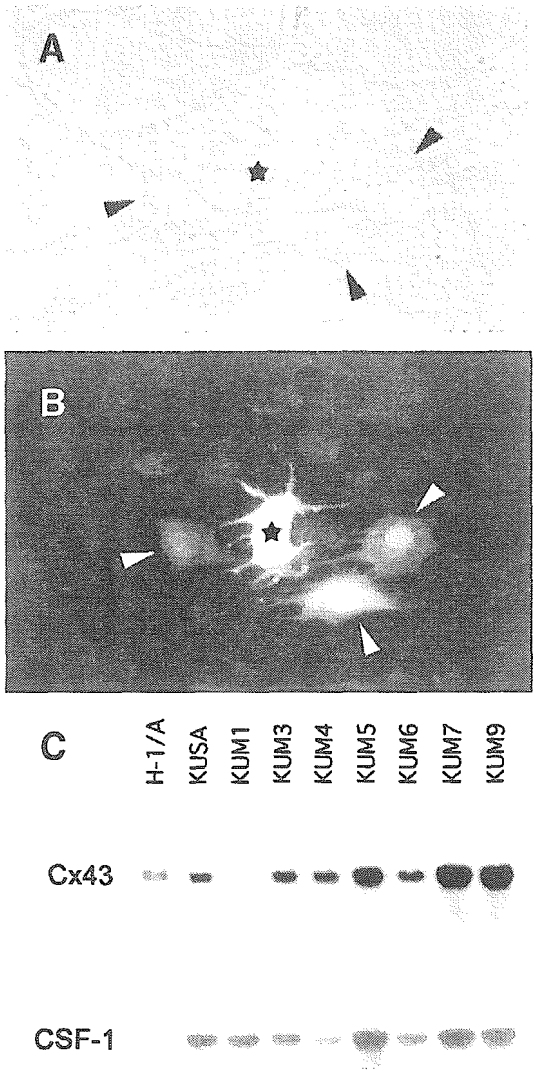

Fig. 4. Dye transfer in KUSA-A1 cells at semiconfluence. Intercellular communication was assessed by the dye transfer method. A and B: Phase-contrast micrograph (A) and fluorescence photograph (B) of KUSA-A1 cells. A KUSA-A1 cell [asterisk] was injected with Lucifer Yellow CH, and the dye was transferred to several adjacent cells. The dye has spread to three first-order-neighboring cells [arrowheads]. (C) Analysis of connexin 43 (Cx. 43) expression by KUSA, KUM1, KUM3, KUM4, KUM5, KUM6, KUM7, and KUM9 cells at semiconfluence. The same blot, which was rehybridized with the CSF-1, is shown for reference [6] in the lower panel.

3.5. Ossification by KUSA-A1 is membranous

To determine whether the ossification by KUSA-A1 is membranous or enchondral, we followed the time-course of KUSA-A1 ossification in the subcutaneous tissue of SCID mice after injecting cells 7 days post-confluence. The injected cells had produced a meshwork of collagen fibers and amorphous ground substance (osteoid matrix) at 1 week (Fig. 6A), and the fibers and ground substance markedly increased and became larger. The matrix was highly calcified at 4 weeks (Fig. 6B and C), and marrow cavities had formed inside the KUSA-A1 bone.

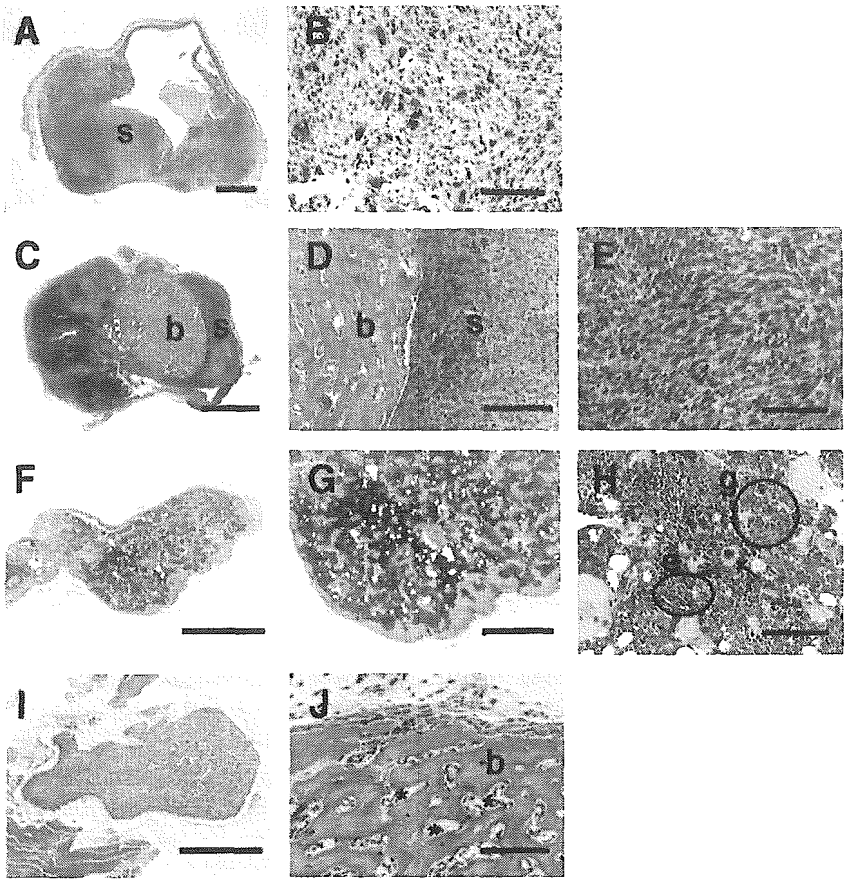

Fig. 5. Microscopic appearance of subcutaneous masses 4 weeks after subcutaneous inoculation of NIH3T3-MTAg (A, B), KUSA-MTAg (C, D, E), KUSA (F, G, H), and KUSA-A1 cells (I, J). (A) Mass of the first type. It is a sarcoma [s] without bone. (B) High-power view of a part of panel (A). The tumor consists of pleomorphic mesenchymal cells, including multinucleated bizarre giant cells. (C, D) Mass of the second type. The mass is composed of sarcoma [s] and well-defined bone [b]. (E) High-power view of part of the tumor in panel (D). The tumor shows proliferation of pleomorphic spindle cells, including giant multinucleated tumor cells. (F, G) Mass of the third type. The mass is composed of complete bone with bone cavities [asterisks], but there is no sarcomatous proliferation. (H) High-power view of part of the mass in panel (G). Trilineage hematopoietic cells (granulocytes [g], erythrocytes [e], and megakaryocyte [arrow]) in the bone cavities inside the mass are shown. (I) Mass of the third type. The mass is composed of complete bone with bone cavities [asterisks], but there is sarcomatous proliferation. (J) High-power view of panel (I). H–E stain. Scale bars: 2 mm (A, C, F, K), 0.5 mm (G), 200 μm (D), and 100 μm (B, E, H, J).

Histological examination of complete bone mass revealed highly dense bone trabeculae, and hematopoietic cells were observed in the bone marrow, as reported previously [6,10]. No cartilage had formed in any of the KUSA-A1-produced bones, indicating that the osteogenesis by KUSA-A1 is membranous ossification rather than enchondral ossification. Osteogenesis was monitored radiographically at scheduled times after the inoculation of $3-5 \times 10^7$ KUSA-A1 cells, and the results showed a gradual increase in newly formed bone 2 weeks after the injection, and complete bone density 4 weeks after the inoculation.

We then monitored the fate of KUSA-A1 bone transplanted into subcutaneous tissue and the abdominal cavity and found that the ectopic KUSA-A1 bone remained unchanged in size and shape for 12 months at both sites. Histological examination revealed complete functional hematopoiesis by ectopic KUSA-A1 bone in the subcutaneous tissue, but not in the abdominal cavity.

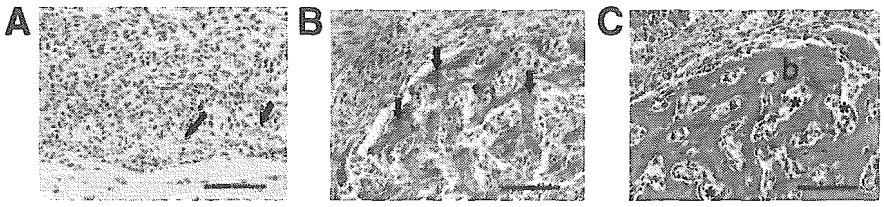

Fig. 6. The process of osteogenesis by KUSA-A1 cells in vivo. (A) One week after the inoculation of 10^7 KUSA-A1 cells, bone formation [arrows] was observed around the periphery of the mass at all inoculation sites. It is noteworthy that no chondrogenesis was observed during early osteogenesis. (B) Two weeks after inoculation. There is more bone matrix [arrows] at week 2 than at week 1. (C) Four weeks after inoculation, the mass consists of complete bone tissue [b] and bone cavities [asterisks]. H–E stain. Scale bars: 100 μm.

4. Discussion

4.1. KUSA-A1 cells can be used as a model for developmental bone formation and abnormal ossification

The sequence of KUSA-A1 bone formation is as follows: deposition of matrix by KUSA-A1 cells that subsequently become mineralized, deposition of bone as a network of immature or woven trabeculae, and formation of bone marrow or conversion of the spongiosa into primary cortical bone by filling of spaces between the trabeculae. This process results in the formation of cancellous bone and bone marrow. Importantly, the osteogenesis by KUSA-A1 cells was irreversible and reproducible, and the transplanted KUSA-A1 cells never transformed into malignant cells, formed any abnormal extracellular matrices, or induced any significant inflammatory reactions. It is noteworthy that the osteogenesis by KUSA-A1 cells was not mediated by chondrogenesis, and it was therefore considered to be membranous ossification. Thus, the unique characteristics of KUSA-A1 cells provide an opportunity to analyze the process of membranous ossification in an experimental system in detail.

In fetal life, primary ossification centers form by one of two processes: endochondral ossification or membranous ossification. Endochondral ossification refers to bony replacement of cartilage and is the mode of formation of the long bones. During membranous ossification, mesenchymal cells form membranes within which ossification occurs, and this is the mode of formation of the scapula and skull and, in part, of the clavicle and pelvis. After birth, bone growth continues by both endochondral and membranous ossification. Further endochondral ossification occurs in the physes and results in continuous longitudinal growth of the long bones until skeletal maturity. KUSA-A1 cells were obtained from a long bone the femur, but formed bone by membranous ossification. There are also cells responsible for the periosteal membranous ossification in tubular bones, which model the diaphyseal cortex, and KUSA-A1 cells may be derived from such a minor cell population in long bones that is responsible for periosteal bone formation or callus.

The process of ossification by KUSA-A1 cells may also serve a model for ectopic or heterotopic ossification, such as soft tissue ossification, ligament ossification, and heterotopic bone formation in a number of disorders, including central nervous system and spinal cord disorders, probably as a consequence of immobilization, a model of myositis ossificans progressiva, which often develops after a traumatic event, and a model of ossification of the posterior longitudinal ligament of the spine, which is characterized by the presence of a linear band of ossification along the posterior margin of vertebral bodies and intervertebral discs, especially in the cervical spine.

4.2. Possibility of implanted-cell transformation

The lack of tumor formation or in vivo transformation after implantation of KUSA-A1 cells into immunodeficient mice does not mean that the donor cells are incapable of transforming after implantation, at least in mice. The observation period after cell implantation into mice is usually less than 1 year because the life span of mice is approximately 2 years. By contrast, since patients who receive cell-based therapy may survive for decades, the possibility of implanted-cell transformation cannot be ignored. Care should be exercised when using donor cells transfected with certain genes for the therapeutic purposes, because zero risk of implanted-cell transformation cannot be achieved, even though human non-tumor cells seldom transform in vitro or in vivo without gene transfection.

4.3. Can cancellous bone grafting be replaced by osteoblast-based therapy?

The transplantation of bone from one site to another usually promotes osteogenesis or provides structural stability. Grafts may be used to fill bone defects, promote union, or provide material for arthrodesis. The donor sites most frequently used for grafts are the iliac crest, tibia, and fibula. Depending on circumstances, the patient or animal may receive either a cancellous bone graft or a cortico-cancellous graft. Cancellous bone grafts are the gold standard for bone defects. They have greater capacity to induce new bone formation and, thus, are considered to be generally much more successful in inducing new bone formation than osteoblast-based therapy. Osteoblast-based therapy is poorer than cancellous bone grafts in providing structural stability.

However, complications occur after cancellous bone grafting and include fracture at the donor site, intraoperative bleeding, and postoperative pain. Graft failure may lead to progressive bone resorption and, ultimately, to disappearance of the graft. Follow-up radiographs show healing of iliac donor sites with sclerosis at the margins of the bone defects. Painful excrescences of the bone may develop at the donor site. Loss of the sharp margins between the graft and host bone on radiographs generally signifies graft healing, and the persistence of a thin residual radiolucent area between the graft and the host bone suggests fibrous union.

It would be interesting to assess the possibility of using mature osteoblasts as a therapeutic agent. The inoculation of isolated mature osteoblasts into a bone defect or fracture site would be a more efficient means of accelerating bone fusion with minimal invasion than inoculation of unfractionated marrow cells into fracture sites. The critical step in realizing osteoblast-based therapy will be the isolation of human counterparts to KUSA-A1 cells and growing them in sufficient numbers in culture. The separation of osteoblasts from human marrow stroma [21] and inoculation of the cells with an appropriate scaffold will provide new methods of

osteogenesis engineering without any of the complications associated with cancellous bone grafts.

Acknowledgements

We would like to express our sincere thanks to Y. Takeda and H. Abe for support throughout the work, and to N. Hida, T. Inomata, Y. Hashimoto, and Y. Nakamura, for providing expert technical assistance. This study was supported by a grant from the Ministry of Education, Culture, Sports, Science, and Technology of Japan, the Health and Labour Sciences Research Grants, and the Pharmaceuticals and Medical Devices Agency to A. U.

References

[1] P. Bianco, P.G. Robey, Marrow stromal stem cells, J. Clin. Invest. 105 (2000) 1663–1668.
[2] M.C. Horowitz, A. Fields, D. DeMeo, H.Y. Qian, A.L. Bothwell, E. Trepman, Expression and regulation of Ly-6 differentiation antigens by murine osteoblasts, Endocrinology 135 (1994) 1032–1043.
[3] E. Canalis, Novel treatments for osteoporosis, J. Clin. Invest. 106 (2000) 177–179.
[4] G.A. Rodan, T.J. Martin, Therapeutic approaches to bone diseases, Science 289 (2000) 1508–1514.
[5] M.F. Pittenger, A.M. Mackay, S.C. Beck, R.K. Jaiswal, R. Douglas, J.D. Mosca, M.A. Moorman, D.W. Simonetti, S. Craig, D.R. Marshak, Multilineage potential of adult human mesenchymal stem cells, Science 284 (1999) 143–147.
[6] A. Umezawa, T. Maruyama, K. Segawa, R.K. Shadduck, A. Waheed, J. Hata, Multipotent marrow stromal cell line is able to induce hematopoiesis in vivo, J. Cell. Physiol. 151 (1992) 197–205.
[7] S. Makino, K. Fukuda, S. Miyoshi, F. Konishi, H. Kodama, J. Pan, M. Sano, T. Takahashi, S. Hori, H. Abe, J. Hata, A. Umezawa, S. Ogawa, Cardiomyocytes can be generated from marrow stromal cells in vitro, J. Clin. Invest. 103 (1999) 697–705.
[8] S. Gojo, N. Gojo, Y. Takeda, T. Mori, H. Abe, S. Kyo, J. Hata, A. Umezawa, In vivo cardiovasculogenesis by direct injection of isolated adult mesenchymal stem cells, Exp. Cell Res. 288 (2003) 51–59.
[9] J. Kohyama, H. Abe, T. Shimazaki, A. Koizumi, K. Kashima, S. Gojo, T. Taga, H. Okano, J. Hata, A. Umezawa, Brain from bone: efficient 'meta-differentiation' of marrow stroma-derived mature osteoblasts to neurons with Noggin or a demethylating agent, Differentiation 68 (2001) 235–244.
[10] K. Ochi, G. Chen, T. Ushida, S. Gojo, K. Segawa, H. Tai, K. Ueno, H. Ohkawa, T. Mori, A. Yamaguchi, Y. Toyama, J. Hata, A. Umezawa, Use of isolated mature osteoblasts in abundance acts as desired-shaped bone regeneration in combination with a modified poly-DL-lactic-co-glycolic acid (PLGA)-collagen sponge, J. Cell. Physiol. 194 (2003) 45–53.
[11] A. Sharov, et al., Transcriptome analysis of mouse stem cells and early embryos, PLoS Biol. 1 (2003) E74.
[12] A. Umezawa, K. Harigaya, H. Abe, Y. Watanabe, Gap-junctional communication of bone marrow stromal cells is resistant to irradiation in vitro, Exp. Hematol. 18 (1990) 1002–1007.
[13] A. Umezawa, J. Hata, Expression of gap-junctional protein (connexin 43 or alpha 1 gap junction) is down-regulated at the transcriptional level during adipocyte differentiation of H-1/A marrow stromal cells, Cell Struct. Funct. 17 (1992) 177–184.
[14] A. Umezawa, K. Tachibana, K. Harigaya, S. Kusakari, S. Kato, Y. Watanabe, T. Takano, Colony-stimulating factor 1 expression is down-regulated during the adipocyte differentiation of H-1/A marrow stromal cells and induced by cachectin/tumor necrosis factor, Mol. Cell. Biol. 11 (1991) 920–927.
[15] H. Sudo, A. Kodama, Y. Amagai, S. Yamamoto, S. Kasai, In vitro differentiation and calcification in a new clonal osteogenic cell line derived from newborn mouse calvaria, J. Cell Biol. 96 (1983) 191–198.
[16] S.B. Doty, B.H. Schofield, Enzyme histochemistry of bone and cartilage cells, Prog. Histochem. Cytochem. 8 (1976) 1–38.
[17] I. Binderman, D. Duksin, A. Harell, E. Katzir, L. Sachs, Formation of bone tissue in culture from isolated bone cells, J. Cell Biol. 61 (1974) 427–439.
[18] P.C. Schiller, G. D'Ippolito, W. Balkan, B.A. Roos, G.A. Howard, Gap-junctional communication is required for the maturation process of osteoblastic cells in culture, Bone 28 (2001) 362–369.
[19] M.M. Saunders, J. You, J.E. Trosko, H. Li, Z. Yamasaki, H.J. Donahue, C.R. Jacobs, Gap junctions and fluid flow response in MC3T3-E1 cells, Am. J. Physiol., Cell Physiol. 281 (2001) C191725.
[20] P.S. Leboy, J.N. Beresford, C. Devlin, M.E. Owen, Dexamethasone induction of osteoblast mRNAs in rat marrow stromal cell cultures, J. Cell. Physiol. 146 (1991) 370–378.
[21] T. Mori, T. Kiyono, H. Imabayashi, Y. Takeda, K. Tsuchiya, S. Miyoshi, H. Makino, H. Matsumoto, H. Saito, S. Ogawa, M. Sakamoto, J-i Hata, A. Umezawa, Combination of hTERT and Bmi-1, E6 or E7 induce prolongation of the life span of bone marrow stromal cells from an elderly donor without affecting their neurogenic potential, Mol. Cell. Biol. 25 (2005) 5183–5195.

Cell Separation Between Mesenchymal Progenitor Cells Through Porous Polymeric Membranes

Akon Higuchi,[1] Yosuke Shindo,[1] Yumiko Gomei,[1] Taisuke Mori,[2] Taro Uyama,[2] Akihiro Umezawa[2]

[1]Department of Applied Chemistry, Seikei University, 3-3-1 Kichijoji Kitamachi, Musashino, Tokyo 180-8633, Japan

[2]Department of Reproductive Biology and Pathology, National Center for Child and Development, Setagaya, Tokyo 154-8567

Received 9 August 2004; revised 5 October 2004; accepted 12 October 2004
Published online 19 May 2005 in Wiley InterScience (www.interscience.wiley.com). DOI: 10.1002/jbm.b.30220

Abstract: This study investigates the separation of two types of marrow stromal cells, KUSA-A1 osteoblasts and H-1/A preadipocytes, by filtration through various porous polymeric membranes. It was found that KUSA-A1 permeates better than H-1/A cells through 12-μm polyurethane foaming membranes. This appears to be due to the relatively smaller cell size of KUSA-A1 cells. In addition, when feed solutions containing suspensions of either cell type or a mixture of the two were used, the permeation ratio was relatively low (< 6%) through polyurethane and surface-modified polyurethane foaming membranes. It was also found that there was some degree of separation between KUSA-A1 and H-1/A cells (separation factor = 1.8) with nylon-net filter membranes, but no separation was obtained when filters made of nonwoven fabrics or silk screens were used. This ability of the nylon-net filter membranes to separate the two cell types was due to a sieving effect that results from an optimal pore size. Finally, permeation of a solution of human serum albumin through the membrane following filtration of the cells did not result in a separation of cells in the recovery solution. © 2005 Wiley Periodicals, Inc. J Biomed Mater Res Part B: Appl Biomater 74B: 511–519, 2005

Keywords: cell separation; mesenchymal progenitor cells; flow cytometry; biomaterials; polyurethane foaming membrane

INTRODUCTION

Bone-marrow stromal cells make up the microenvironment of the bone marrow and are required for the generation of multipotent stem cells.[1] In addition, bone-marrow stromal cells have many characteristics of mesenchymal stem cells, which produce progeny that can differentiate into multiple cell lineages. Pluripotent stem cells derived from marrow stroma can differentiate into several cell types, including bone, cartilage, fat, tendon, and muscle. Recent studies also show that the marrow stroma may be a potential source of cardiomyocytes.[2]

Purification and isolation of specific mesenchymal cells are necessary to obtain bone-marrow stromal cells for use in clinical applications. For example, it is necessary to generate cardiomyocytic progenitors from marrow stroma for the treatment of heart failure by cell transplantation into damaged myocardia. Thus, a method is needed for the separation and isolation of specific mesenchymal cells from bone-marrow stromal cells. Cell separation can be accomplished by centrifugation,[3,4] fluorescence-activated cell sorting (FACS),[5] magnetic cell selection,[6–9] affinity chromatography,[10,11] or membrane filtration.[12–14] Of these methods, membrane filtration method is a good candidate for the purification of mesenchymal cells because it is simple and inexpensive and because it is easy to maintain sterility during the filtration process. In fact, a previous study[14] showed that $CD34^+$ cells could be purified by filtration through chemically modified 5-μm-pore polyurethane (PU) membranes.

Here the separation of cells from a mixture of KUSA-A1 and H-1/A cells with the use of membrane filtration is reported. The goal of this study was to find the optimal membrane type (membrane pore size, morphology, and material) and filtration conditions for the isolation of marrow stromal cells.

MATERIALS AND METHODS

Materials

Base membranes used for the chemical modification were porous PU foaming membranes (Ruby Cell S, Toyo Polymer Co., Ltd.). Porous PU foaming membranes containing 0.61% of epoxy group (PU-epoxy) were prepared by plasma polymerization with glycidylmethacrylate after the membranes were plasma discharged at 200 W for 30 s under 0.2 torr of Ar gas.[14] The average pore size of the PU

Correspondence to: Akno Higuchi (e-mail: higuchi@ch.seikei.ac.jp)
Contract grant sponsor: Ministry of Education, Culture, Sports, Science, and Technology of Japan Grant-in-Aid for Scientific Research on Priority Areas (B, "Novel Smart Membranes Containing Controlled Molecular Cavity"); contract grant number: 13133202
Contract grant sponsor: Salt Science Foundation
Contract grant sponsor: Asahi Glass Foundation

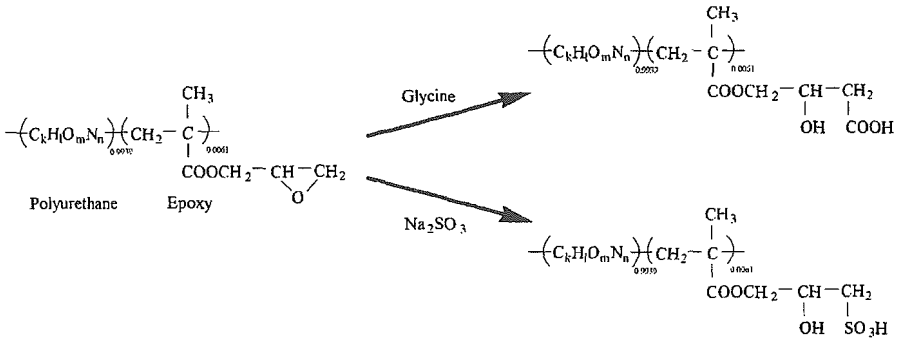

Scheme 1

and PU-epoxy membranes evaluated from capillary flow porometer measurements (Porous Materials, Inc.) was 12 μm. The PU and PU-epoxy membranes had 86% porosity and 1.2-mm thickness.

Nylon-net filters [NY11 (pore size = 11 μm), Millipore Corporation], two kinds of nonwoven fabrics having fine fiber diameter for cleaning lenses made of acrylonitrile (Cleaning lens, No Brand Co.) and nylon + polyester (La Clean, 3052-01, Nagoya Glass Co.), and silk screens made of silk (No. 150, Nihon Zokei Co.) and Tetron™ (Nos. 150 and 250, Nihon Zokei Co.) were also used for the cell separation, where "No." indicates number of fibers per inch.

Human serum albumin (HSA, 019-10503, Wako Pure Chemical Industries) was used as received. Cell Tracker Orange™ (C-2927, Molecular Probes, Inc.) and Cell Tracker Green™ (C-2925, Molecular Probes, Inc.) were used as received. Other chemicals, purchased from Tokyo Chemical Co., were reagent grade and were used without further purification. Ultrapure water was used throughout the experiments.

Preparation of Surface-Modified Membranes

Sulfonic acid and carboxylic acid groups were introduced from the opening reaction of the epoxy group on the PU-epoxy membranes, followed by the reaction between the epoxy group and H_2SO_4 or glycine reported in the literature.[14–16] Reaction conditions are reported in the literature.[14] The product anticipated to result from the ring-opening reaction of the epoxy group is shown in Scheme 1.[14] The resultant membranes were referred to as PU-SO_3H and PU-COOH membranes. After the reaction, the surface-modified PU membranes were rinsed in ultrapure water for 3 h, and stocked in ultrapure water at 4°C.

Cell Culture

Mesenchymal progenitor cell lines, KUSA-A1 and H-1/A, derived from the bone marrow of C3H/He and C57/Bl mice, respectively,[1,2] were maintained in DMEM media (D5648, Sigma-Aldrich, Japan K.K.) supplemented with 100 mg/L streptomycin sulfate (196-08511, Wako Pure Chemical Industry, Ltd.), 70 mg/L benzylpenicillin potassium (023-07731, Wako Pure Chemical Industry, Ltd.) and 10% fetal bovine serum (FBS, JRH Bioscience). KUSA-A1 and H-1/A cells were expanded by standard cell culture techniques[17–19] in 75-cm^2 tissue-culture flasks containing 40 mL of 10% serum-supplemented medium in a CO_2 incubator (BNA-111, Espec Co.) in 5% CO_2 atmosphere at 37°C.

The cell number was characterized by observation of the cells with an inverted microscope (Diaphoto TMD300, Nikon Co.) equipped with a CCD video camera, ARGUS 20 (Hamamatsu Photonics K.K.) and a temperature-regulated box.

Cell Dying with Cell Tracker

KUSA-A1 cells and H-1/A cells were dyed with Cell Tracker™ (Cell Tracker Orange™ and Cell Tracker Green™, respectively) in order to mark each cell in flow-cytometry analysis. A quantity of 1 mg Cell Tracker Orange™ was dissolved in 1 mL of methanol, and the Cell Tracker Orange™ solution was aliquotted into 20 samples (50 μL). A quantity of 50 μg Cell Tracker Green™ was dissolved in 0.5 mL of dimethylsulfoxide, and the Cell Tracker Green™ solution was aliquotted into 10 samples (50 μL). The Cell Tracker Orange™ and Cell Tracker Green™ solutions were stored under −20°C. The cell dying with Cell Tracker Orange™ and Cell Tracker Green™ was performed as follows:

1. A quantity of 50 μL of Cell Tracker solution was pipetted into 5 mL of 10% serum-supplemented DMEM medium.
2. The medium was decanted off, and the cells were rinsed with 10 mL phosphate-buffered solution (PBS).
3. The PBS was decanted off and the Cell Tracker™ solution was pipetted into the tissue-culture flask. The cells in the tissue-culture flask were incubated in a 5% CO_2 atmosphere for 30 min at 37°C.
4. The Cell Tracker™ medium was decanted off and the cells were subsequently rinsed with a quantity of 10 mL PBS solution. Twenty milliliters of 10% serum-supplemented DMEM medium was pipetted into the tissue-culture flask after the PBS solution was decanted off, and the cells in the tissue-culture flask were again incubated in a 5% CO_2 atmosphere for 30 min at 37°C.
5. Step 4 was performed in duplicate.
6. After incubation, the DMEM medium was decanted off and a quantity of 10 mL PBS solution was added to the tissue-culture flask in order to rinse the cells.
7. A quantity of 4 mL of trypsin in PBS solution was pipetted into the tissue-culture flask after the PBS solution was decanted off. After 5 min, the trypsin solution was decanted off and a quantity of 5 mL of DMEM medium was added to the tissue-culture flask. The cells on the bottom of the culture flask were resuspended in the DMEM medium by gently pipetting up and down.
8. The cell suspension was centrifuged at 130 rpm for 3 min. The supernatant was carefully decanted off, and 7 mL of fresh DMEM medium was added to the cells.

9. The cell suspension was gently pipetted up and down to resuspend cells on the bottom of the centrifuge tube, and the cell density was counted with the use of flow cytometry (Coulter EPICS™ XL, Beckman-Coulter Co.).

Cell Permeation

KUSA-A1 cells and H-1/A cells were inserted into the centrifugation tube containing DMEM medium. Each cell density was adjusted to be 50,000 cells/mL by the addition of DMEM medium. The single- or mixed-cell solution of 6 mL containing KUSA-A1 cells and/or H-1/A cells was permeated through the membranes with the permeation apparatus described in the previous study.[14] The diameter of the membrane was 25 mm and filtration rate was 1 mL/min. The number of each cell of KUSA-A1 cells and H-1/A cells in the permeate and feed solutions (N_p and N_f, respectively) was counted from the flow-cytometry measurements.

The permeation ratio is defined as

$$\text{permeation ratio } (\%) = (N_p/N_f) \times 100. \quad (1)$$

After the cell filtration, the membrane was upside down inside the membrane holder, and 0.5-wt % HSA solution of 6 mL was permeated through the membrane with the use of the same membrane and the apparatus at filtration speed of 1 mL/min to remove the attached cells on the membrane and to collect them in the HSA solution. The recovery ratio is defined as

$$\text{recovery ratio } (\%) = (N_r/N_f) \times 100, \quad (2)$$

where N_r is the number of cells in the permeate solution after the permeation of HSA solution. The filtration experiments were performed at 25±0.5°C.

The membranes used in the cell filtration were unmodified PU membranes, surface-modified PU membranes, nylon-net filters, nonwoven fabrics, and silk screens. The permeation experiments of cells were performed on each membrane with four independent membranes.

Flow-Cytometric Analysis of Cells

The size and shape of KUSA-A1 cells and H-1/A cells were analyzed from forward light scattering and side light scattering of laser beam (Ar laser, 488 nm) by flow cytometry. The number of KUSA-A1 cells and H-1/A cells in the feed and permeate solutions was analyzed from flow-cytometric scattergrams of KUSA-A1 cells and H-1/A cells in the fluorescent intensity at 575 and 525 nm.

SEM Analysis of Cells on the Membranes

After permeation of suspended cell solution through the membranes, the membranes were rinsed with saline. Consequently, the membranes were treated with 3-wt % glutaraldehyde in saline for 2 days at 4°C. The samples were washed with saline, subjected to a drying process by being passed through a series of graded-alcohol–saline solutions (0, 25, 50, 75, and 100%) and dried in a vacuum for 10 h at room temperature.[20] The dried membranes were gold coated and examined with the use of a JSM-5200 scanning electron microscope (SEM, JEOL, Ltd.).

RESULTS AND DISCUSSION

Flow-Cytometric Analysis of Cells

KUSA-A1 osteoblasts and H-1/A preadipocytes, two mesenchymal cell lines, were incubated with fluorescent probes (Cell Tracker Orange™ and Cell Tracker Green™, respectively) to allow their independent detection before and after permeation through porous polymeric membranes. The numbers of KUSA-A1 and H-1/A cells in the mixed cell solution were determined from flow-cytometric scattergrams at 575 nm for KUSA-A1 cells and 525 nm for H-1/A cells. These values are close to those of phycoerythrin (PE) and fluorescein isothiocyanate (FITC), which are used for conventional cell-counting of specific cells.[21] Figure 1(a) shows the flow-cytometric scattergrams for the KUSA-A1 and H-1/A cells. The fluorescence intensities at 525 and 575 nm for the two cell types were significantly different. The forward and side light scattering intensities, shown in Figure 1(b), indicate that both cell types have a broad size distribution, although KUSA-A1 cells are mostly smaller than H-1/A cells. Furthermore, the flow-cytometric scattergrams of KUSA-A1 cells and H-1/A cells (forward light scattering intensity vs. side light scattering intensity and fluorescence intensity at 525 nm vs. 575 nm) were found to be identical in single- and mixed-cell solutions (data not shown). Thus, cell aggregates did not appear to be formed when KUSA-A1 cells and H-1/A cells were mixed together in DMEM medium.

Cell Separation Through PU Membranes

The differences in the cell sizes and shapes suggested that KUSA-A1 and H-1/A cells can be separated by using porous polymeric membranes. This possibility was examined with the use of a variety of membrane types. Figure 2 shows an SEM image of the surface of the porous polymeric membranes tested in this study. A regular screen pore morphology was found on the surface of nylon-net filters [Figure 2(b)] and silk screens [Figure 2(e,f)], whereas a specific pore morphology was not found on the surface of nonwoven fabrics [Figure 2(c,d)]. Furthermore, a deformed open pore structure was found on the surface of the PU membranes used in this study [Figure 2(a)].

The permeation of cells through PU and surface-modified PU membranes was investigated first, because a previous study showed that hematopoietic stem cells can be recovered from peripheral blood with the use of surface-modified PU (PU-COOH) membranes.[14] The permeation of KUSA-A1 cells, H-1/A cells, and a mixture of the two cell types through PU and surface-modified PU membranes (pore size = 12 μm) at 25°C was examined. Figure 3(a) shows the permeation ratio through the membranes with a suspension of a single cell type (50,000 cells/mL) used as the feed solution, and Figure 4(a) shows the results obtained when the feed solution was a mixture of the two cell types. A relatively low (< 6%) permeation ratio through PU and surface-modified PU membranes was found with either a single-cell solution or a mixed-cell solution. Because open pore volume of the

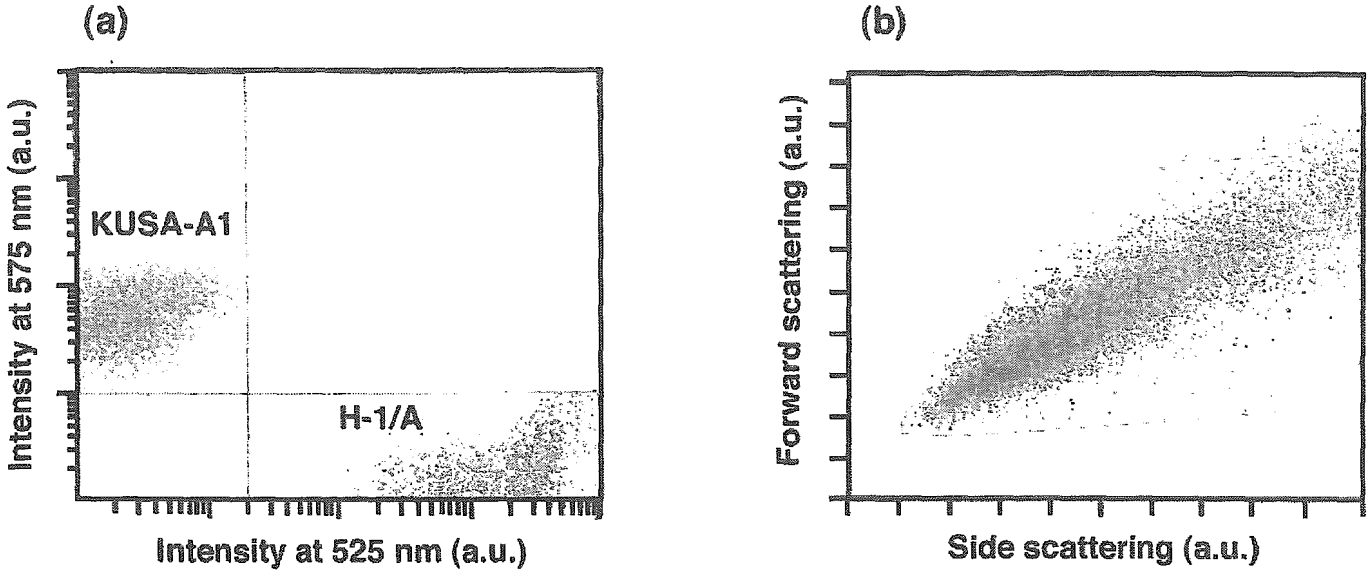

Figure 1. Flow-cytometric scattergrams of mixed solution of KUSA-A1 cells (orange dots) and H-1/A cells (green dots), each having a cell density of 50,000 cells/mL in the fluorescent intensity at 575 nm and 525 nm (a) and in the light intensity of forward scattering and side scattering (b). [Color figure can be viewed in the online issue, which is available at www.interscience.wiley.com.]

membrane interior in PU and surface-modified PU membranes is calculated as 0.506 mL (i.e., 1.25 cm × 1.25 cm × 3.14 × 0.12 cm × 0.86) and total cell volume permeated through the membranes is approximately calculated as 3.375×10^{-4} mL in a mixed-cell solution [i.e., 6 mL × 50,000 cells/mL × 2 × (7.5×10^{-4} cm × 7.5×10^{-4} cm ×

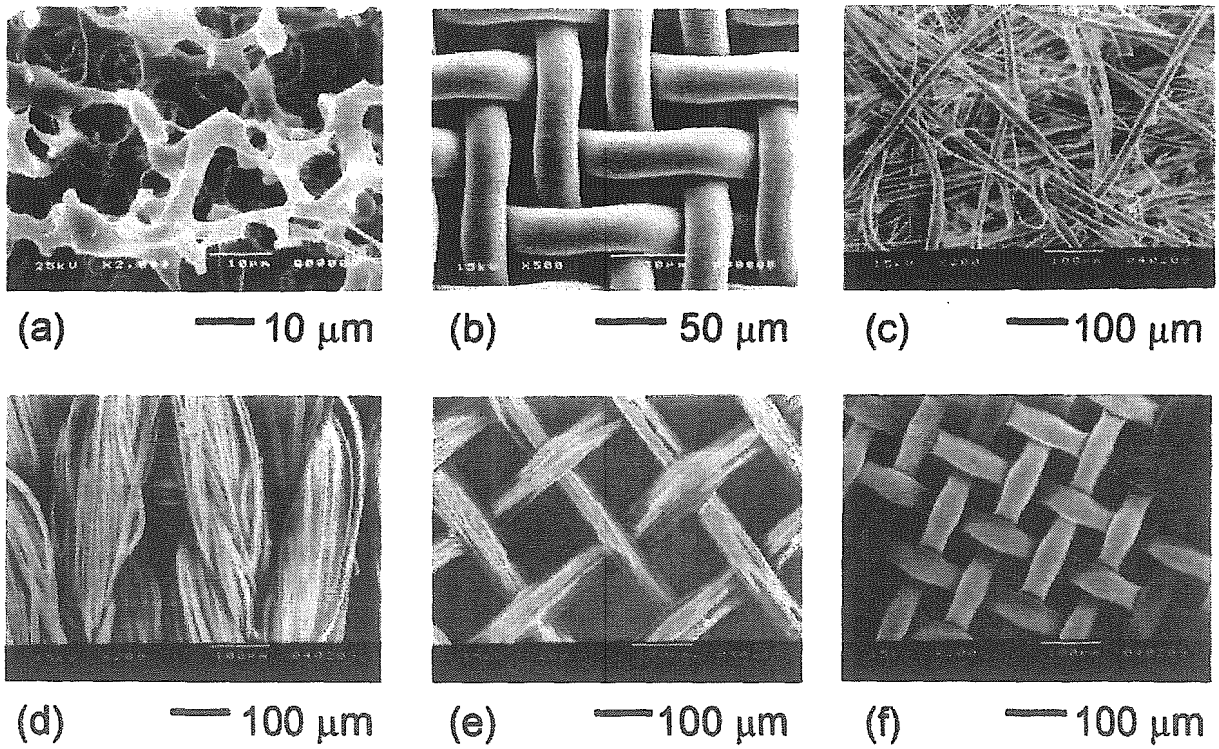

Figure 2. Scanning electron micrographs of the membrane surfaces of (a) unmodified PU membranes, (b) nylon-net filter, (c) nonwoven fabrics made of acrylonitrile, (d) nylon + polyester, (e) silk screens made of silk mesh size 150), and (f) silk screens made of Tetron™ (mesh size 250).

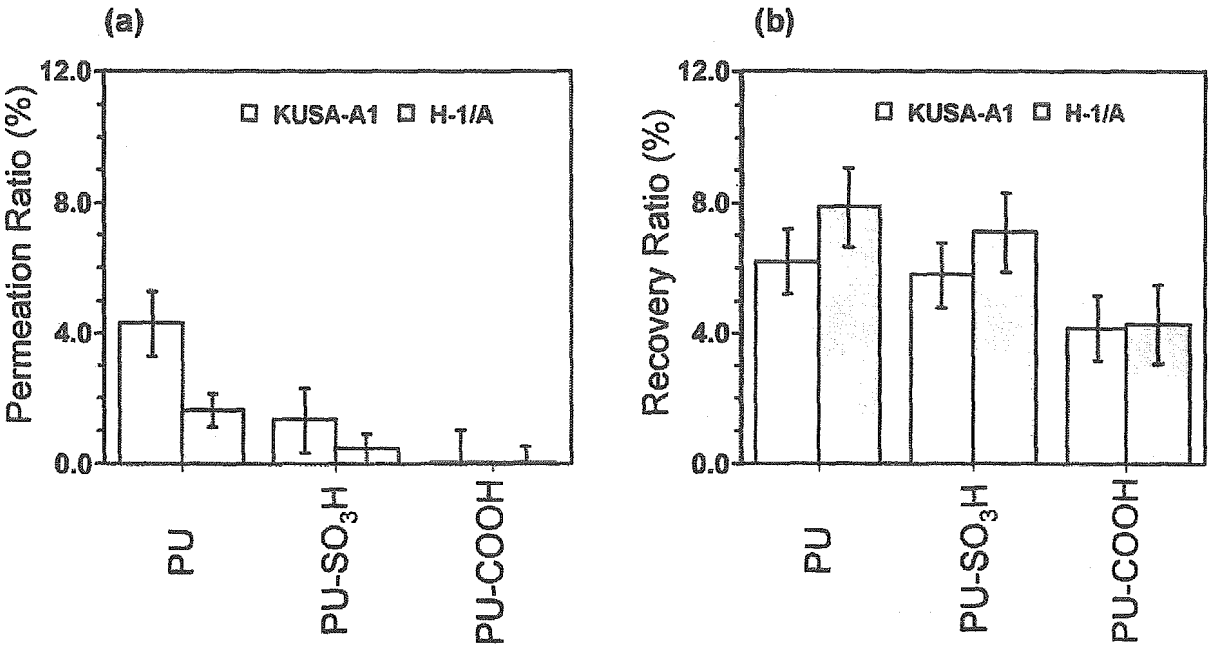

Figure 3. Permeation ratio (a) and recovery ratio (b) of KUSA-A1 cells and H-1/A cells through PU, PU-SO_3H, and PU-COOH membranes after permeation of single-cell solution at the cell density of 50,000 cells/mL and 25°C. Data are expressed as the means ± standard deviation of four independent measurements.

7.5×10^{-4} cm × 4/3)] in this study, the low permeation ratio is not due to the overloading of the cells permeated through the membranes. The low permeation ratio through PU and surface-modified PU membranes is due to high degree of cell adhesion on the membranes and a complicated pore structure of the membranes.

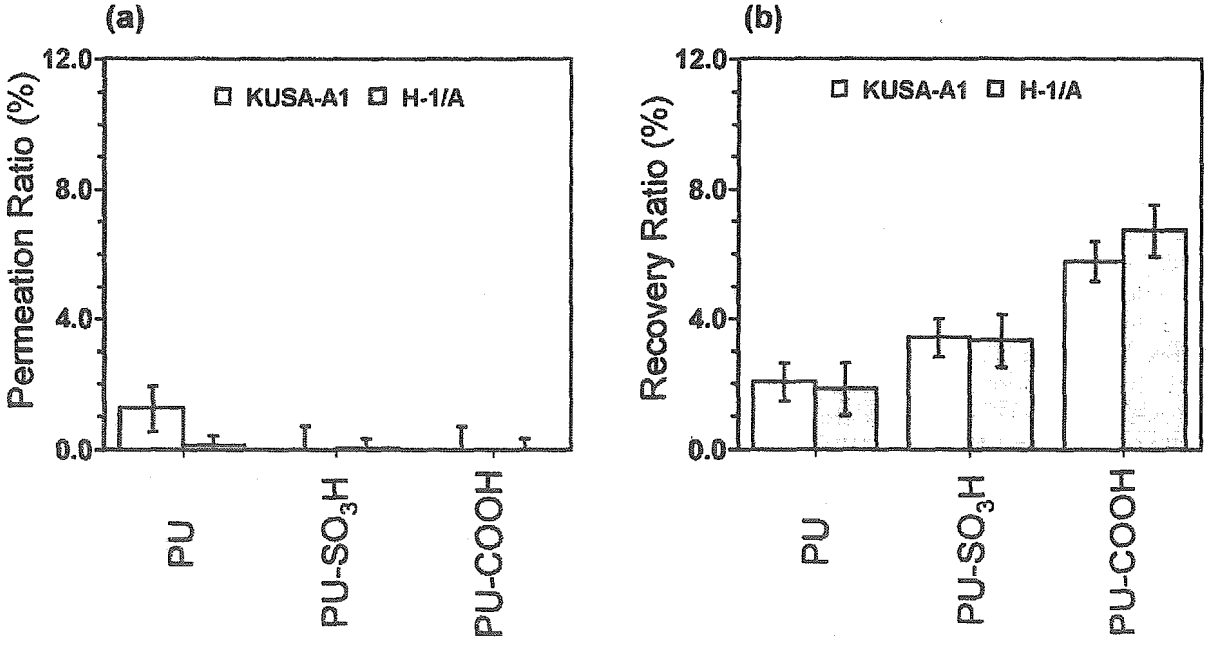

Figure 4. (a) Permeation ratio and (b) recovery ratio of KUSA-A1 cells and H-1/A cells through PU, PU-SO_3H, and PU-COOH membranes after permeation of mixed-cell solution at a cell density of 50,000 cells/mL each and 25°C. Data are expressed as the means ± standard deviation of four independent measurements.

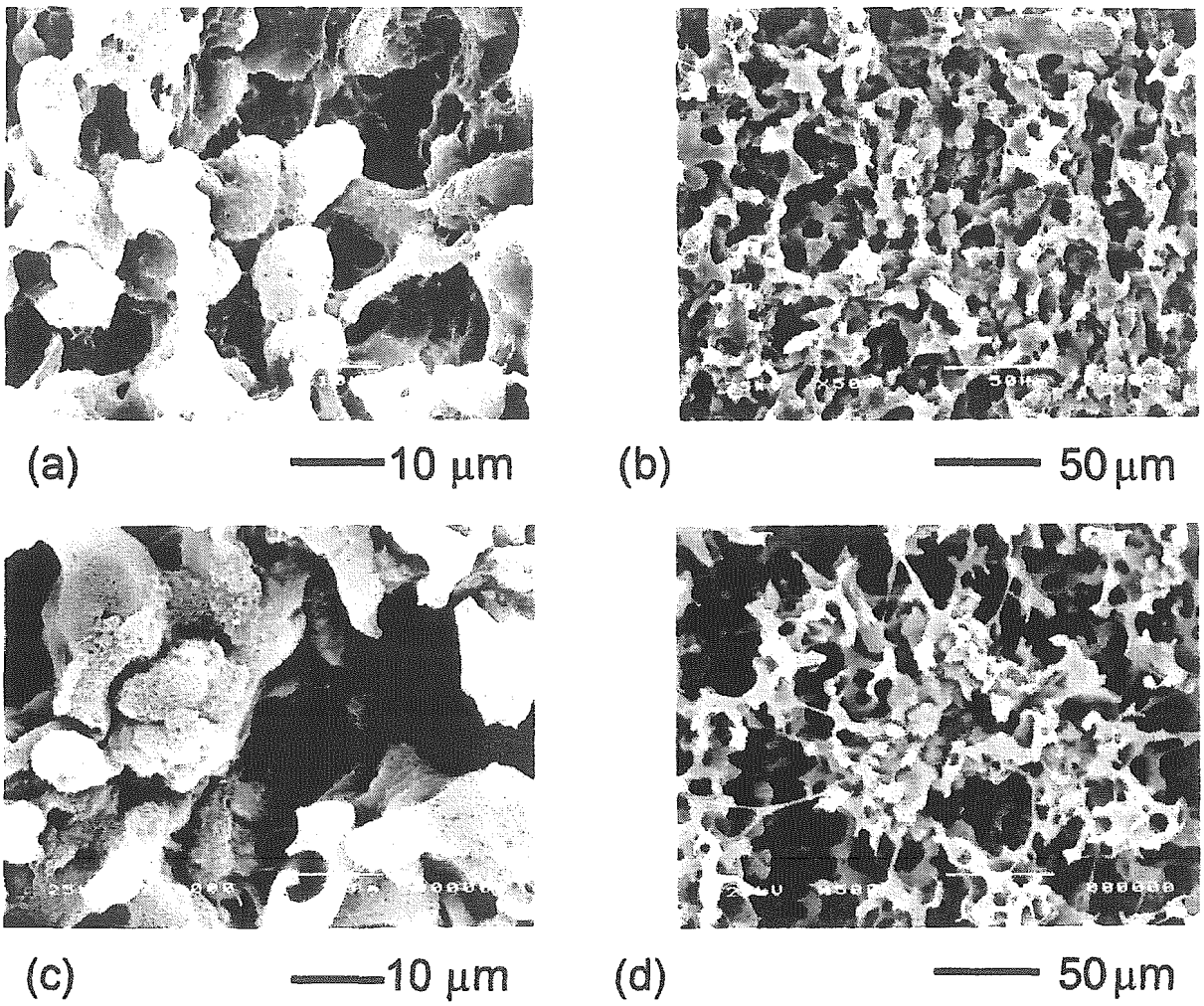

Figure 5. *Scanning electron micrograph of membrane surface of unmodified PU membranes after permeation of KUSA-A1 cells (a), (b) or H-1/A cells (c), (d) at the cell density of each 50,000 cells/mL and 25°C.*

The permeation ratio of both KUSA-A1 and H-1/A cells through PU membranes was found to be higher than that through PU-SO_3H and PU-COOH membranes. The surface modification of PU-SO_3H and PU-COOH membranes may cause the decreased pore size of the surface-modified membranes compared to the unmodified PU membranes. The permeation ratio when the feed solution contained a single cell type was found to be higher than the permeation ratio when it was a mixed-cell solution through PU and surface-modified PU membranes. Although FACS analysis suggested that coagulation or interaction does not occur between KUSA-A1 and H-1/A cells (data not shown), some coagulation or interaction between KUSA-A1 and H-1/A cells that was not detected from FACS analysis might lead to a decrease of the permeation ratio in the mixed-cell solution compared to the permeation ratio in the single-cell solution. It was also found that the permeation ratio for KUSA-A1 cells was higher than for H-1/A cells, which is consistent with the relatively smaller size of KUSA-A1 cells, as found in Figure 1(b).

Figure 5 shows a SEM image of the PU membrane surface after the permeation of KUSA-A1 or H-1/A cells. There was extensive adhesion of the KUSA-A1 and H-1/A cells to the membrane surface. The high adhesiveness of the cells may explain their low permeation ratios through the PU membranes. SEM images also revealed that the size of KUSA-A1 cells was similar to that of H-1/A cells (approximately 10 to 15 μm in diameter).

Next the effect of passing a HSA solution through the membranes following permeation of the single-cell or mixed-cell solutions was examined. Figures 3(b) and 4(b) show that the recovery ratio of KUSA-A1 and H-1/A cells following this treatment was higher than the permeation ratio. However, the recovery ratio was still below 10% through any of the PU membranes. Slightly higher recovery ratio through the PU and PU-SO_3H membranes in a mixed feed solution was found when compared to that in a single-cell type. On the other hand, no significant difference in recovery ratio was found between feed solutions containing a single cell type or a mixture of cell types through PU-COOH membranes.